AFRL-IF-RS-TR-2005-329
Final Technical Report
November 2005

SONICFLIP: AN INTEGRATED PLATFORM FOR BIOFLUID MONITORING

Cornell University

Sponsored by
Defense Advanced Research Projects Agency
DARPA Order No. J302/52

APPROVED FOR PUBLIC RELEASE; DISTRIBUTION UNLIMITED.

AIR FORCE RESEARCH LABORATORY
INFORMATION DIRECTORATE
ROME RESEARCH SITE
ROME, NEW YORK

STINFO FINAL REPORT

This report has been reviewed by the Air Force Research Laboratory, Information Directorate, Public Affairs Office (IFOIPA) and is releasable to the National Technical Information Service (NTIS). At NTIS it will be releasable to the general public, including foreign nations.

AFRL-IF-RS-TR-2005-329 has been reviewed and is approved for publication

APPROVED: /s/

THOMAS E. RENZ
Project Engineer

FOR THE DIRECTOR: /s/

JAMES A. COLLINS, Deputy Chief
Advanced Computing Division
Information Directorate

REPORT DOCUMENTATION PAGE

Form Approved
OMB No. 074-0188

1. AGENCY USE ONLY (Leave blank)	2. REPORT DATE	3. REPORT TYPE AND DATES COVERED
	NOVEMBER 2005	Final Feb 03 – Feb 04

4. TITLE AND SUBTITLE
SONICFLIP: AN INTEGRATED PLATFORM FOR BIOFLUID MONITORING

5. FUNDING NUMBERS
C - F30602-03-2-0035
PE - 63739E
PR - E117
TA - 00
WU - 75

6. AUTHOR(S)
Amit Lal

7. PERFORMING ORGANIZATION NAME(S) AND ADDRESS(ES)
Cornell University
115 Day Hall
Ithaca New York 14853

8. PERFORMING ORGANIZATION REPORT NUMBER
N/A

9. SPONSORING / MONITORING AGENCY NAME(S) AND ADDRESS(ES)
Defense Advanced Research Projects Agency
3701 North Fairfax Drive
Arlington Virginia 22203-1714

AFRL/IFTC
26 Electronic Parkway
Rome New York 13441-4514

10. SPONSORING / MONITORING AGENCY REPORT NUMBER
AFRL-IF-RS-TR-2005-329

11. SUPPLEMENTARY NOTES
AFRL Project Engineer: Thomas E. Renz/IFTC/(315) 330-3423/ Thomas.Renz@rl.af.mil

12a. DISTRIBUTION / AVAILABILITY STATEMENT
APPROVED FOR PUBLIC RELEASE; DISTRIBUTION UNLIMITED.

12b. DISTRIBUTION CODE

13. ABSTRACT *(Maximum 200 Words)*
The SonicFlip project created technologies that enable microfluidic integration at a wristwatch scale with Complimentary Metal Oxide Semiconductor, CMOS, electronics compatible voltages and currents. The architecture included a CMOS chip driving an array of piezoelectric actuators. By driving the actuators at different phases, we achieved pumping and mixing. Since each pixel was under electronic control, programmable forces were achieved inside microfluidic channels. A fabrication method was developed to create pillars of magnetic materials between the Lead-Zirconate-Titanate, PZT, and the silicon structure. Novel methods were developed to acoustically separate beads by sizes in an optically observable aperture. A unique flow sensor paradigm using viscous drag on a beam inside a flow channel was invented and implemented. This flow sensing method is scalable to nano-scale and mimics beam flow sensing used by micro and millimeter scale biological cells and insects.

14. SUBJECT TERMS
Microfluidics, Piezoelectric Actuators, Interstitial Fluid Measurement

15. NUMBER OF PAGES
50

16. PRICE CODE

17. SECURITY CLASSIFICATION OF REPORT	18. SECURITY CLASSIFICATION OF THIS PAGE	19. SECURITY CLASSIFICATION OF ABSTRACT	20. LIMITATION OF ABSTRACT
UNCLASSIFIED	UNCLASSIFIED	UNCLASSIFIED	UL

Table of Contents

List of Figures

List of Tables

Summary

The goals of this project were to develop a technology to enable highly integrated microfluidic systems in a watch-like assay format. Boundary conditions included 3-5 volt battery operation for 1-2 week missions of interest, (biofluid monitoring of warfighters on missions with a potential threat from chemical or biological warfare agents). In order to meet the specifications we investigated the use of piezoelectric actuators for both direct current force generation and ultrasonic field generation in microfluidics utilizing acoustic streaming and radiation forces. In addition to technology development for integrated microfluidics, we also delivered ultrasonic interstitial fluid sampling and protein assays based on detecting cytokines and CRP (C-reactive proteins). Modeling of the effect of ultrasonic forces on micro-particles with the inclusion of thermodynamic Brownian motion was conducted to optimize and investigate the limitations of ultrasonic nonlinear forces on molecular and/or bead mixtures. The effect of GHz (Giga Hertz) radiation on microfluidics was conducted to investigate RF (Radio Frequency) and ultrasonic molecule simulation.

A PZT/Si/PDMS (Lead Zirconate Titanate/Silicon/ Polydimethylsilane), sandwich microfluidic framework has been sufficiently worked out to justify serious pursuit. In this paradigm, a PZT chip was laser micromachined (a technology developed in this project) to include pixels, cantilevers, and springs which are driven by CMOS (Complimentary metal Oxide Semiconductor) amplifiers. Secondly, a silicon chip including flow sensors, membranes, and surface micromachines is bonded to the PZT chip. On top of the silicon chip will be a PDMS/plastic, cap to form the microchannels. Below are highlights for this project, broken up into sections:

1: PZT Array for Programmable Microfluidic Actuation: This work included processing to tune PZT pixel arrays for obtaining resonant frequency matching between pixels. Bonding technology to attach PZT arrays to pc-boards and pogo pin arrays was developed.
Electronics control of a 2D (2 Dimensional) piezoelectric pillar array at micro-power requires frequency independent phase shifters and low voltage electronics. A gate array solution to generate sine and cosine signals up to 3 MHz, (Mega Hertz) for digital control of pixels was developed. Additionally, the PI (Principal Investigator) taught an analog circuit design class and included the analog op-amp array design as a class project, resulting in 10 man-year design effort accomplished in one semester. A process flow was developed to drive 2D PZT arrays by CMOS from the bottom, leading in the future to a CMOS controlled PZT array.
2: Quadrature Sine Wave Generator: This work included development of vortex particle concentration for sensor applications. Modeling was used to optimize the basic technology and papers were published.

3 Microfluidic Actuator for Fluid Mixing: This section offered new results in the polysilicon structure ultrasonic excitation inside microchannels leading to vortex particle collection.

4 Flow Sensor Integrated in Microfluidic Channel: An integrated cantilever drag flow sensor that led to the analytical model development and fabrication procedure to add high-aspect ratio technology into the microfluidic technology is described.

5 Elastic Feedback System for Needle Insertion and Fluid Sampling: A platform for insertion of microneedle arrays or single needle with elastic feedback for a more natural insertion is described. The work will lead to an optimized micromachined framework. This structure was transitioned to another project, at Becton Dickinson, on pigs, for ISF (Interstitial Fluid) sampling. Further work has led to the development of microprobes for sample collection and potential measurements.

6 Ultrasonic Separations and Pumping in Glass Capillary System: The glass-capillary/PZT technology was used to first focus and then separate by size, beads in the channels, using ultrasonic mode control of the capillary and the PZT. An analytical model that predicts a path to optimization was developed.

7 Separation of Microparticles Using an Ultrasonic Standing Wave Field: Modeling of ultrasonic separation, including Brownian diffusion, to investigate the limits of ultrasonic particle separations was developed

8 Sensing Protein Conformational Changes With Resonant Antennas: The object of this subproject was to investigate the effect of protein content on Radio Frequency, RF, transmission through microfluidic channels. The promising results may lead to content based proteomics in future devices.

1 PZT Array for Programmable Microfluidic Actuation

For the SonicFlip system, a two dimensional microfluidic system was needed to actuate fluid through various channels where the contents of the fluid can be checked. This task was accomplished through the implementation of a two dimensional PZT pixel array. Each pixel in the array can be driven with different frequencies, amplitudes, and phases, to produce an infinite number of acoustic field gradients. One advantage of this approach is that with acoustic streaming, disposable microfluidic cassettes of any material can be used with any liquid.

A PZT plate was developed with grooves, which define the individual pixels, cut into it. A holder with pogo pins was designed to make electrical contact but still allow for motion in the PZT, (**Figure 1.1**). Each pixel was driven at the same resonant frequency and amplitude, but with variations in phase. This simplified the circuitry because only two driving signals were needed: sine and cosine. Many different acoustic field gradients can be created with this design by changing the phase of one pixel.

The circuitry implementing this strategy was built. Frequency independent phase shifters were shown to work at frequencies above 14 MHz (Mega Hertz). The computer controlled cross point switch allowed the user to determine the phase for each pixel. This system allowed fluid flow testing on top of the PZT pixel array, (**Figure 1.2**).

Results
Work focused on characterization of the flow on top of the pixel array and determination of velocity based on variations in the signal amplitude. Motion of 17 μm microspheres placed in the fluid was measured. The particle velocity was 122 μm/s for a peak to peak voltage of only one volt (Vpp). Particle velocities of 1.65 mm/s were obtained with 3 Vpp. The velocity-amplitude followed an expected square relationship. **Figure 1.3** shows the relationship between velocity and signal amplitude.

Laser trimming was used where all pixels could be tuned to the same resonant frequency, eliminating small variations in resonant frequencies for the pixels in the area, (**Figure 1.4)**. Removing material from a pixel raises its resonant frequency. It was shown that ten cuts with a 40 mW, (milli Watt) laser increased the resonant frequency 15 kHz (kilo Hertz), (**Figure 1.5**). Additionally, the impedance of the transducer decreased, an indication of a lower loss resonator. Damage the PZT by excessive laser power would increase its impedance.

The Cornell Nano Fabrication Facility was used to fabricate a two-dimensional PZT array, with dimensions down to 40x40 microns, connected to an underlying electrode array. This electrode array could be on a CMOS chip in the future. The ultrasonic response from each pixel was highly reproducible and matched within 0.5% across an array.

Future Work

Future work will involve smaller PZT pixels and possible schemes for connection to the controlling circuitry. Microfluidic channels in PDMS, which can be placed on top of the PZT array, are also being tested. Challenges include acoustic coupling of the PDMS to the PZT.

Characterization of the PZT pixel motions should also be investigated. An interferometer setup can be used to examine the motion on top of the array. Mathematical models should also be made that can simulate the acoustic fields created by the pixels.

Digital sine wave generation was developed and should be combined in the future with the phase shifter circuitry for a stand alone phase control system for the array.

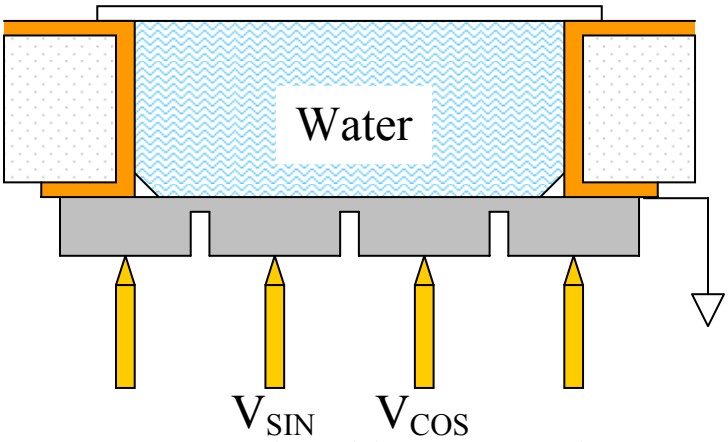

Figure 1.1 PZT Plate Design

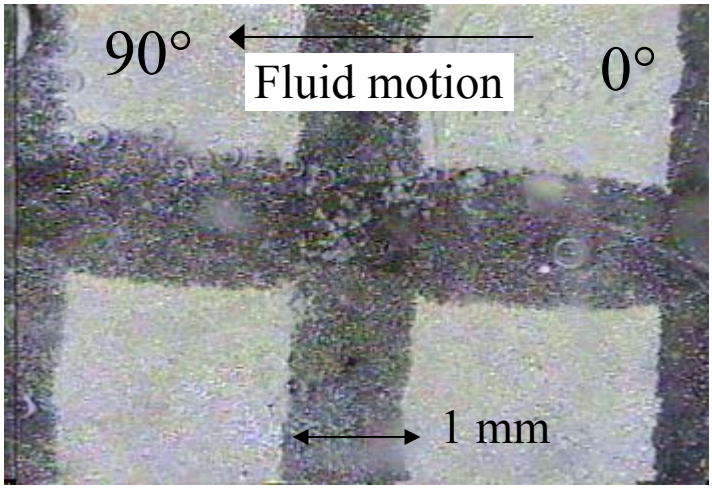

Figure 1.2 Cross point Switch on PZT

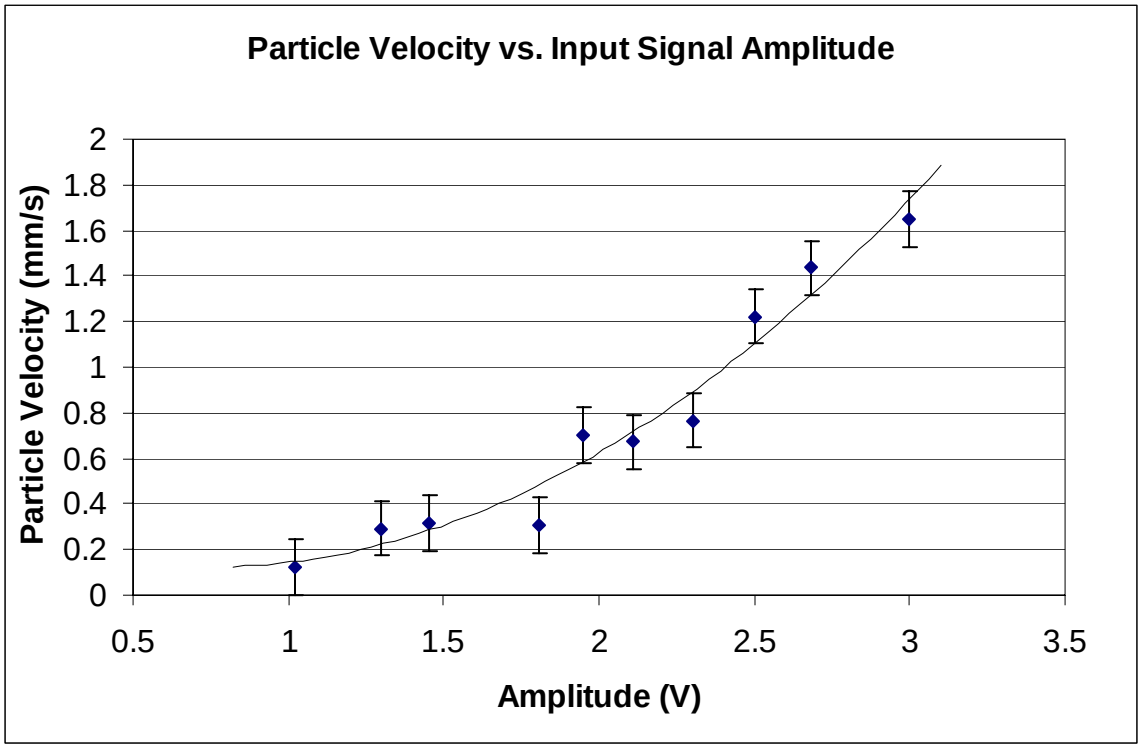

Figure 1.3 Velocity versus Input Signal Amplitude for Acoustic Streaming

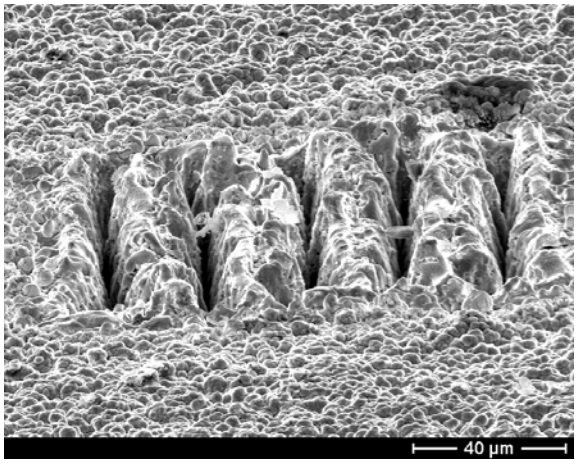

Figure 1.4 Laser Trimming to Vary Resonant Frequency

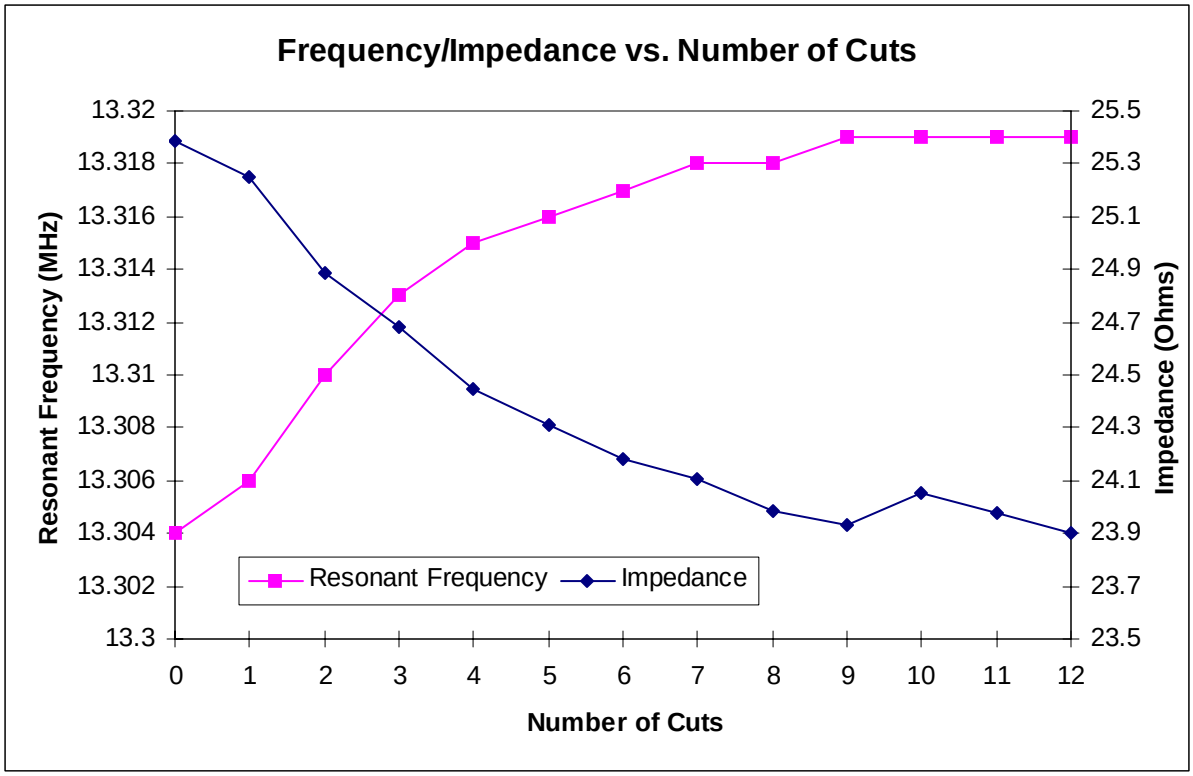

Figure 1.5 Resonant Frequency versus Number of Laser Cuts

2 Quadrature Sine Wave Generator

Due to the requirements of the phase shifter circuit for the PZT pixel array, a quadrature sinusoidal wave generator was needed to create four sine waves with phases 0, 90, 180, and 270 degrees. In addition, the frequencies created must cover a large bandwidth, from 100 kHz to 15 MHz, so that different resonant frequencies can be excited. The frequency should be changed in increments as small as 100 Hz.

This goal has been nearly achieved using the Xilinx Spartan2 Field Programmable Gate Array, FPGA, which is programmed by the XSA100 circuit board from XESS, (**Figure 2.1**). Using the Direct Digital Synthesis (DDS) module from Xilinx, a sine and cosine wave generator was created. The DDS module created the lookup tables and the counters that make this possible.

These digital outputs were connected to digital-to-analog converters from Analog Devices (AD7127). Because complementary outputs were created, the two digital FPGA outputs became four analog signals with two DACs (Digital to Analog Converter), (**Figure 2.2**).

Results
The prototype created four sinusoid waves with a maximum frequency above 2.5 MHz, (**Figure 2.3**). Above that, there was more quantization error, which gave the wave the appearance of steps, rather than a pure curve, (**Figure 2.4**). The minimum frequency was 800 Hz, which is also the frequency resolution. Power consumption was measured to be 2 W for the entire system.

Future Work
The maximum frequency could be increased by increasing the input clock frequency to the FPGA and optimizing the internal layout of our circuit in the FPGA,. Another possible solution would use the Virtex2 FPGA from Xilinx, which can handle higher clock frequencies.

To improve the frequency resolution, more input bits can be added, but this can affect the maximum frequency. Optimized layout can also reduce these effects. Filters and amplifiers can be added to reduce noise and quantization error.

Power consumption can be reduced as well, but must be done in such a way as to not lose speed. Lastly, a microcontroller is planned to control of the entire system. The microcontroller will control the FPGA inputs and process the FPGA outputs with a counter circuit and then provide closed loop feedback control. An additional LCD (Liquid Crystal Display) display would give an interface for an easy to use standalone system to provide input signals with different phases.

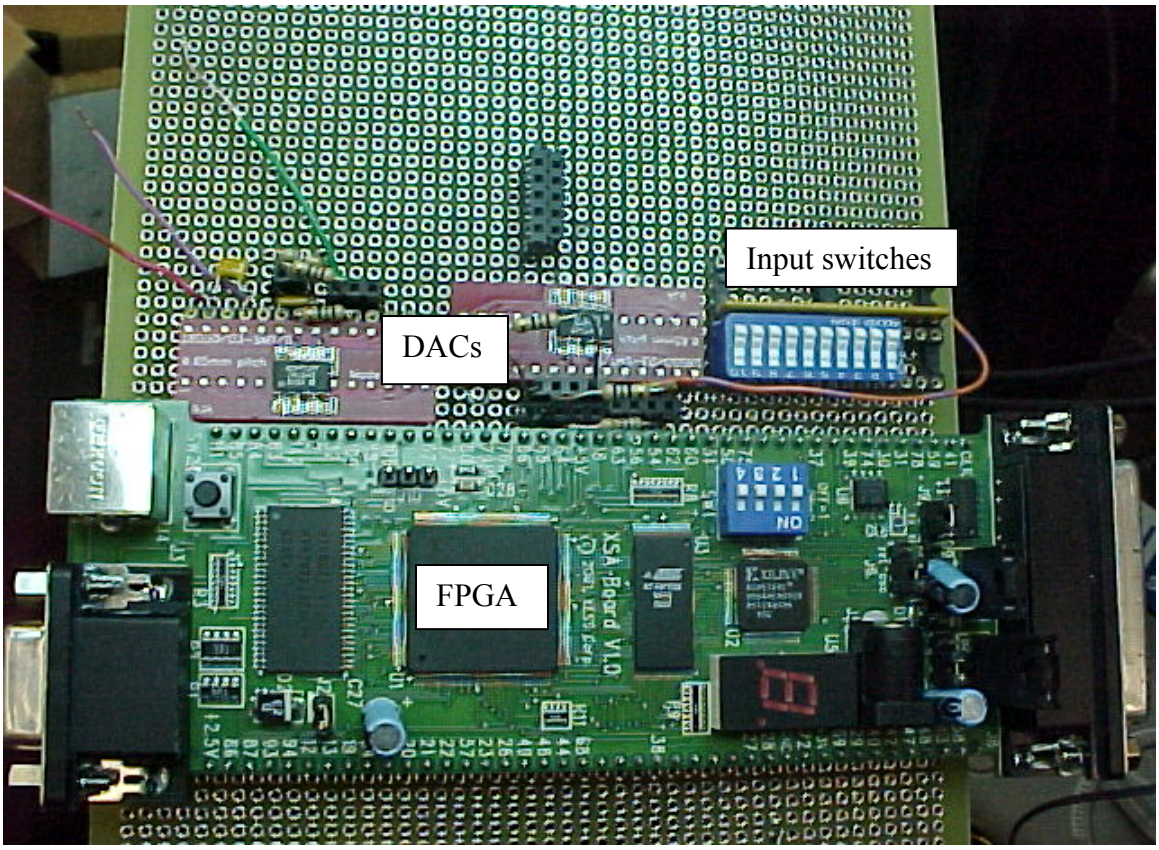

Figure 2.1 XSA Circuit Board with FPGA

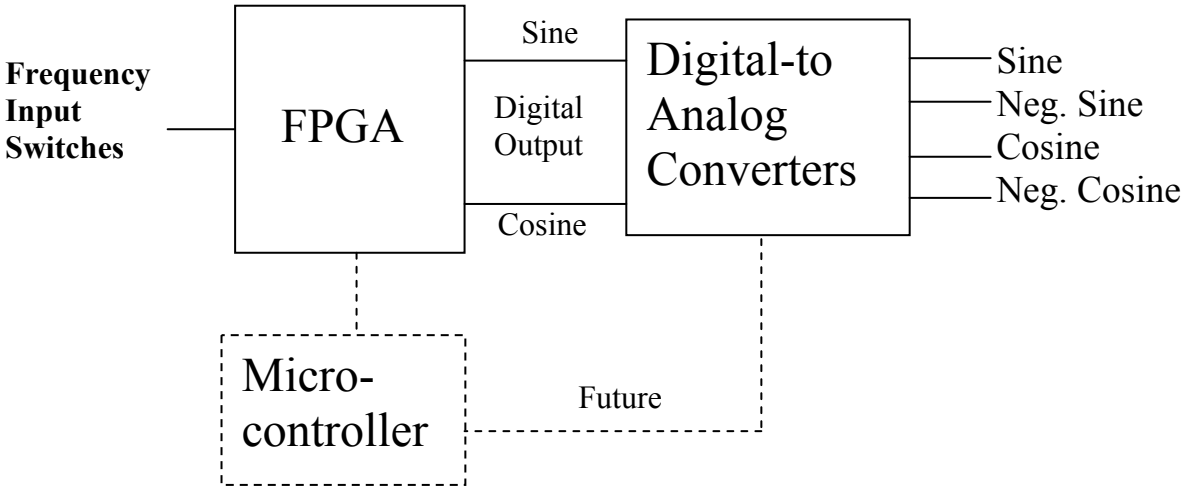

Figure 2.2 Digital to Analog Output Diagram

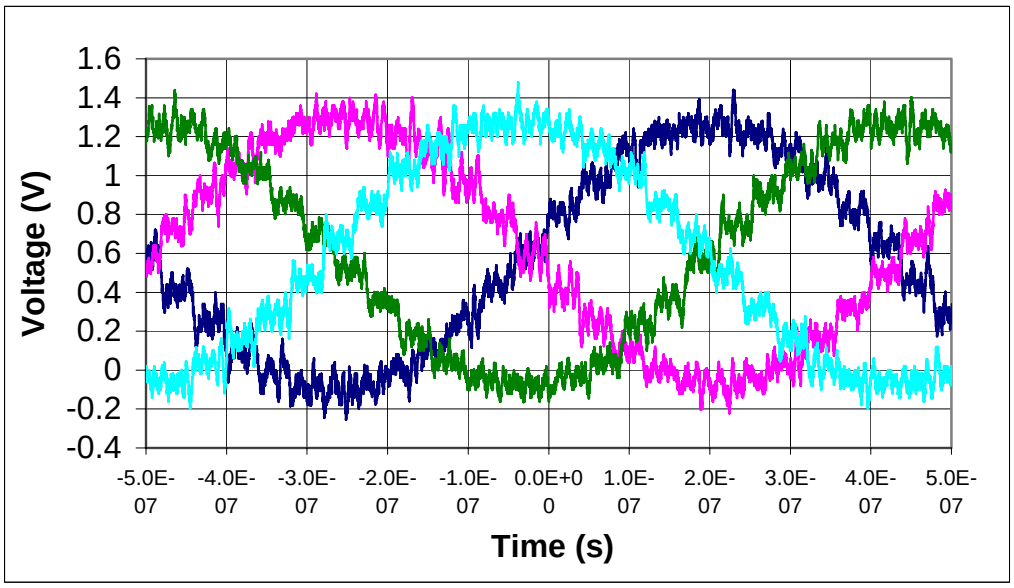

Figure 2.3 Output Signal at Frequency = 1.04 MHz

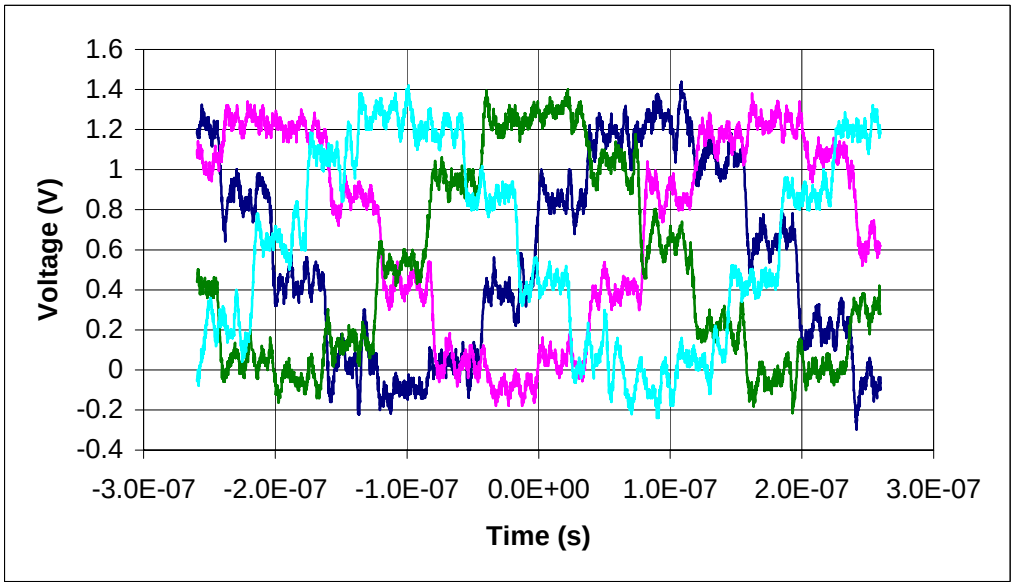

Figure 2.4 Output Signal at Frequency = 2.53 MHz

3 Microfluidic Actuator for Fluid Mixing

The goal of this sub-project was to design and fabricate a microfluidic actuator for fluid mixing and particle entrapment diagramed in **Figure 3.1-Figure 3.4**. **Figure 3.5** shows a SEM (Scanning Electron Micrograph) of a disk actuator. Specific accomplishments were:

- A microfluidic actuation paradigm was developed and it achieved addressable fluid actuation over a wide frequency range (100 kHz ~ 10 MHz).
- Fluid actuation was obtained by a single PZT die at the back of a Si (Silicon) sample, a structure that is simple, potentially inexpensive and consumes little power.
- A variety of fluidic effects were observed in a fluidic channel with an effective Reynolds's number of 0.1.A raw computational fluid dynamics simulation model was created for fluid flow around resonating microstructures inside a microfluidic channel.
- New devices with cornered actuator geometries (triangle, pentagon, hexagon) were designed to ascertain and verify the effect of actuator geometry on fluid vortex formation.
- To overcome a stiction problem with the use of SU-8 photoresist during sample release, the new devices have more etch-holes, reducing the release time down from ~20 minutes to less than 5 minutes.
- A process flow was developed for a device with SU-8 walls and Teflon-heat shrink cap (giving a variable height inside the channel).

Vibrating hubs with shielded coaxial cables were fabricated underneath the hub for capacitive captured particle detection, **Figure 3.6**. As shown in **Figure 3.6**, the detection apparatus used the effect of a captured bead on the capacitance fringing field of the plates to detect and report on the presence of beads.

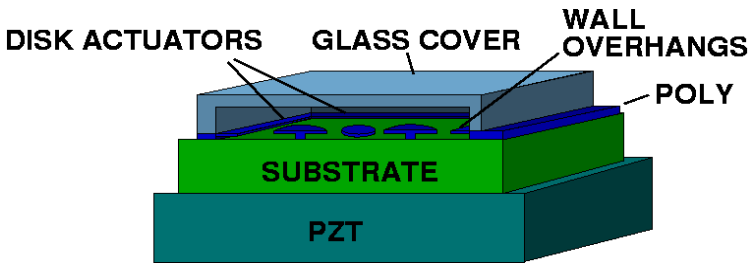

Figure 3.1 Microfluidic Actuator

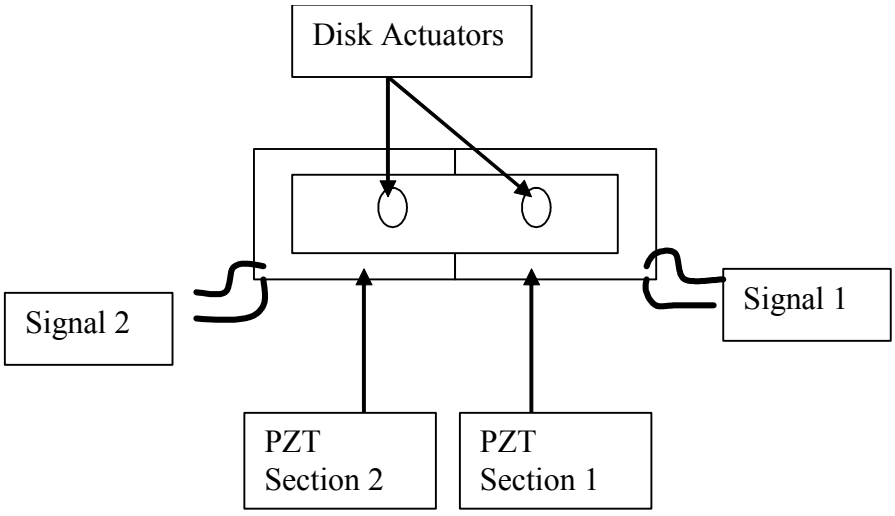

Figure 3.2 Top View of Actuator Structure

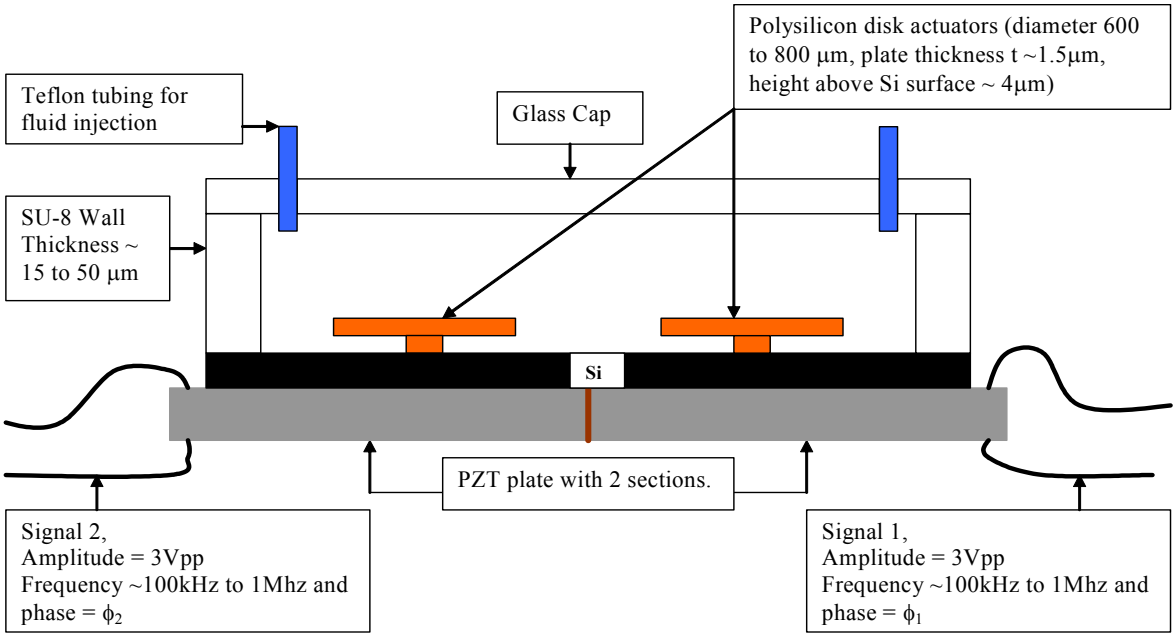

Figure 3.3. Side View of Actuator Structure with Glass Cap

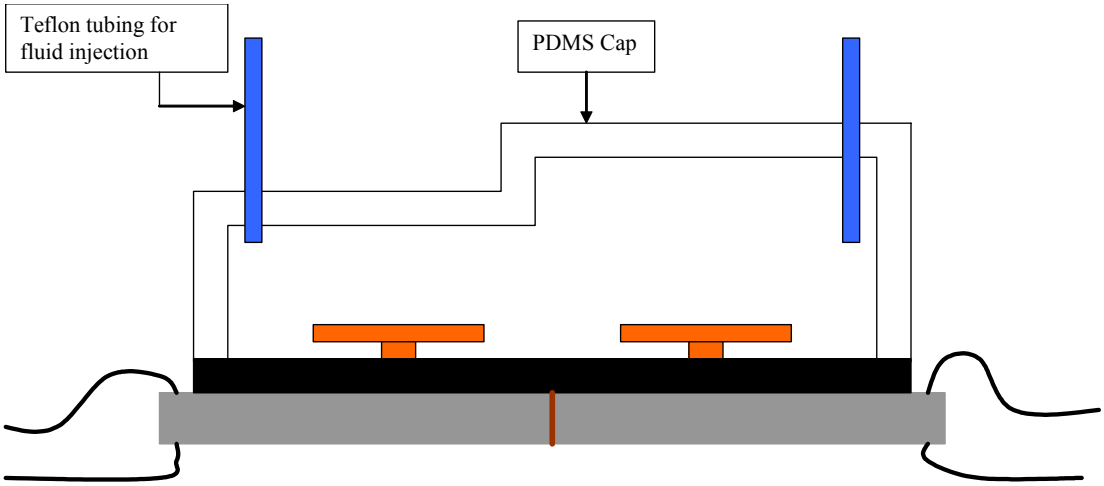

Figure 3.4 Side View of Actuator Structure with PDMS Cap

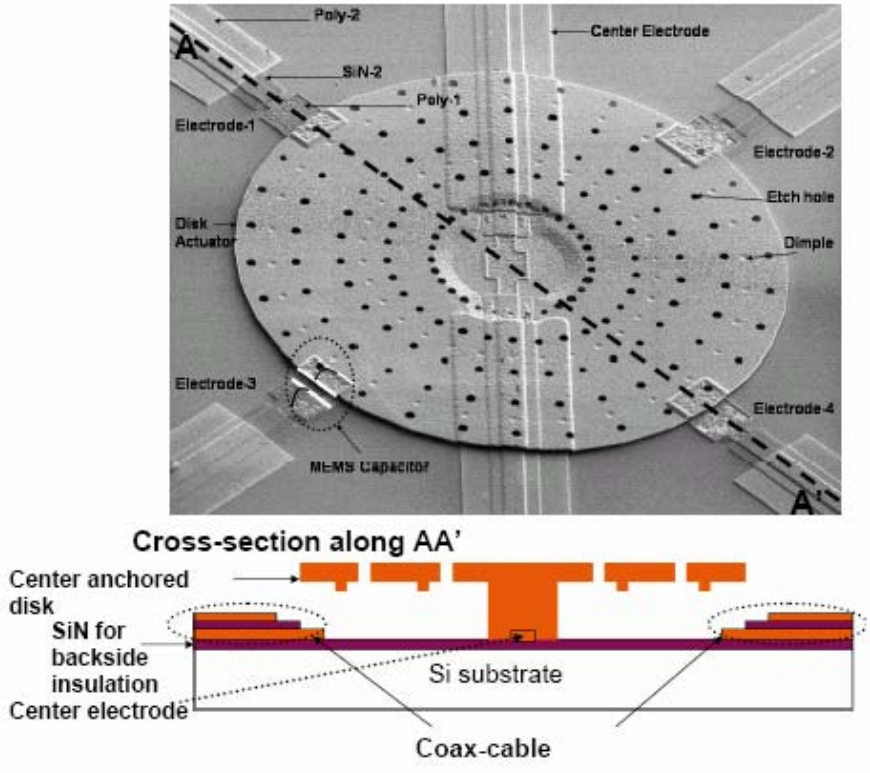

Figure 3.5 SEM of Actuator Structure and Cross Section View

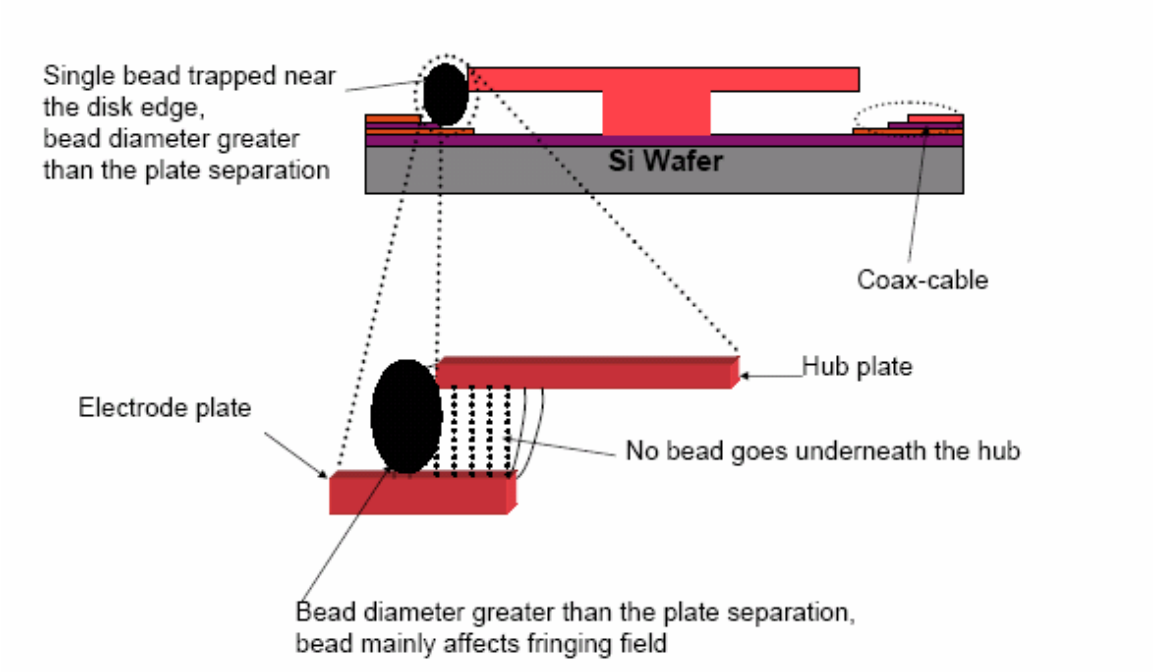

Figure 3.6 Filter Operation of Actuator Structure

4 Flow Sensor Integrated in Microfluidic Channel

Flow sensors were integrated inside the microfluidic channel to enable flow characterization with an array of flow sensors as well as to provide feedback control of the flow. A process flow was developed to fabricate the structure with a nickel cantilever. The six mask process flow is described in **Figure 4.1(a-h)**. For low Reynolds number flow ($Re << 1$), viscous forces dominated inertial forces. This flow sensor measured flow using the drag forces in a direction transverse to the direction of flow in the channel. The flow sensor consisted of a cantilever beam, anchored at the upstream end, placed at a small angle to the direction of flow as shown in **Figure 4.2**.

The beam divided the channel into unequal parts (1 & 2) causing different flow profiles in the two parts. This caused two different pressure gradients (P1 & P2) on the two sides of the beam, causing a net force, transverse to the direction of flow. This force may cause a deflection of the beam for a flexible beam or cause a net moment 'M' translated to the anchor in the case of rigid beams. Flow can be sensed by measuring either the tip displacement of the beam or the stress in the anchor using a piezoresistive bridge network as described later.

Analytical Model: An analytical model developed for the flow sensor is summarized in **Figure 4.3**.

Experimental verification of principle using plastic devices: A proof of concept with plastic devices was demonstrated (fabricated by Stereo Lithography at Becton Dickinson). **Figure 4.4** shows a plastic device with input and output fluidic ports.

Results

2D and 3D models for flow around microbeams were developed using the CFDRC (Computational Fluid Dynamics Research Corporation) design tool. Simulated values matched experimental results from the plastic devices. The results are shown in **Figure 4.5**. Using simulations, the stress distribution underneath the anchor was obtained. These results were used to design piezoresistive layout underneath the anchor to sense the flow. Design of peizoresistors using simulation results – mask design: An example of a layout is shown in a SEM of the layout in **Figure 4.6**.

Future work

- Resist thickness – Currently, molds of resist thickness up to 20 microns to electroplate nickel are used. This can be increased by multiple coats of the resist to create thicker nickel for stiffer beams.

- While using gold etchant to release the cantilevers, chromium (which is part of the seed layer) is attacked vigorously. Other metals or photoresists will be investigated for future sacrificial layers.

- Closed loop control of flow using the output of the piezoresistive network should be developed to provide dynamic control.

Cross Section **Top View**

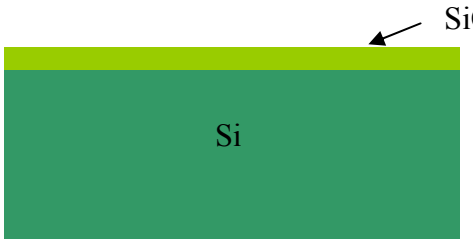

(a) Deposit polysilicon, implant, and pattern. Evaporate Al (5000 Å) and form interconnects.

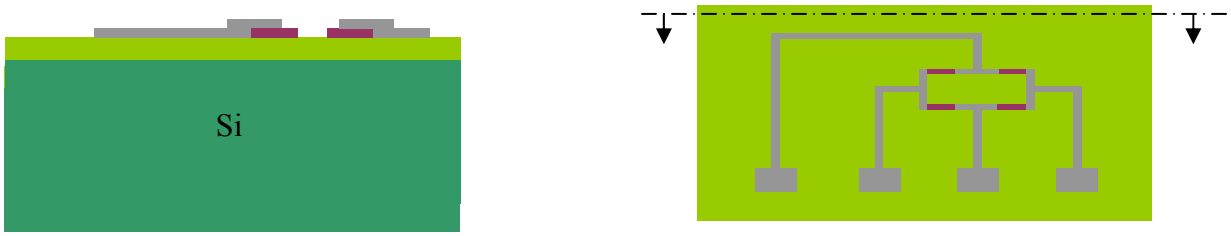

(b) Silicon oxide (5000 Å). This will provide isolation of the underlying circuitry from the channel.

(c) Top view (right) shows dotted regions corresponding to the area in which silicon oxide is etched away to access the Al contact pads

(d) A seed layer of Cr/Cu/Cr for Ni electroplating is formed using a liftoff step.

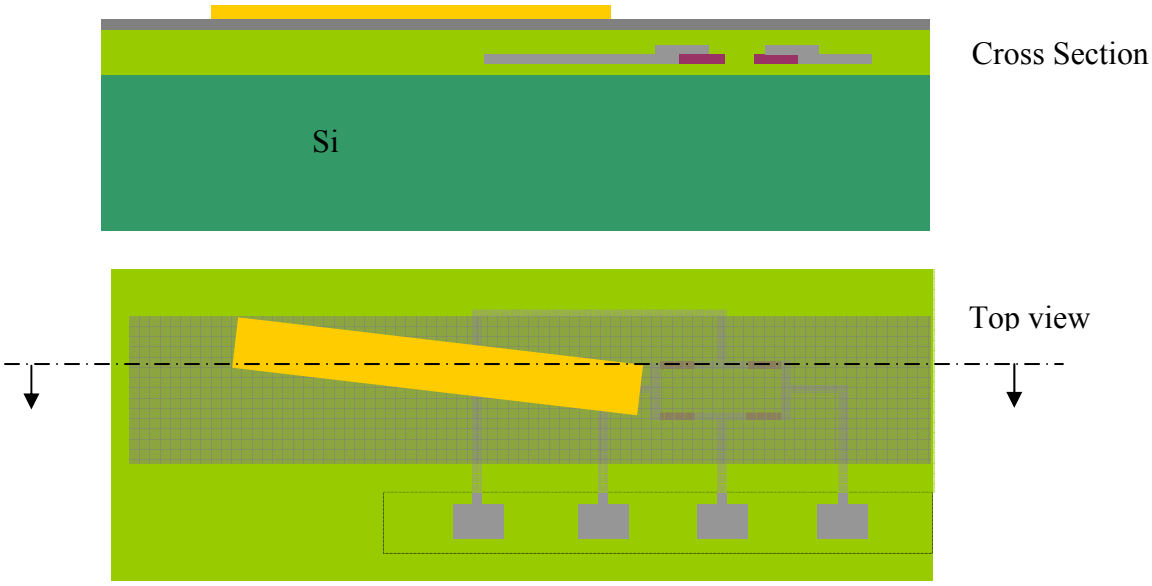

(e) A 3000 Å gold layer is formed as a sacrificial layer to release the nickel cantilever

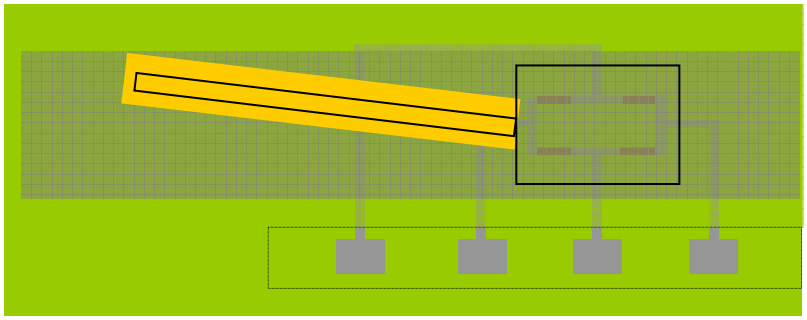

(f) A mold is then patterned over the seed layer such that the cantilever part of the mold lies over the gold sacrificial layer.

(g) Nickel electroplating to form the cantilevers

(h) Cantilevers are released by etching the sacrificial gold layer

Figure 4.1. Fabrication Processing Flow continued

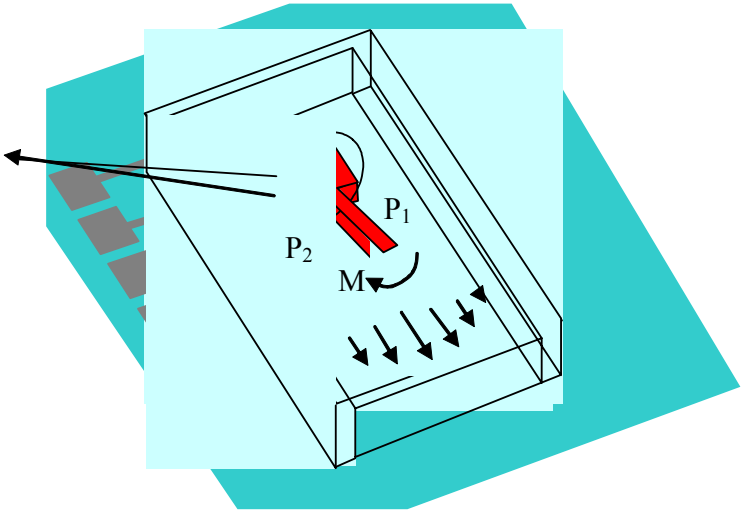

Figure 4.2 Micro- Electrical Mechanical System Cantilever Beam in Microchannel Flow Field

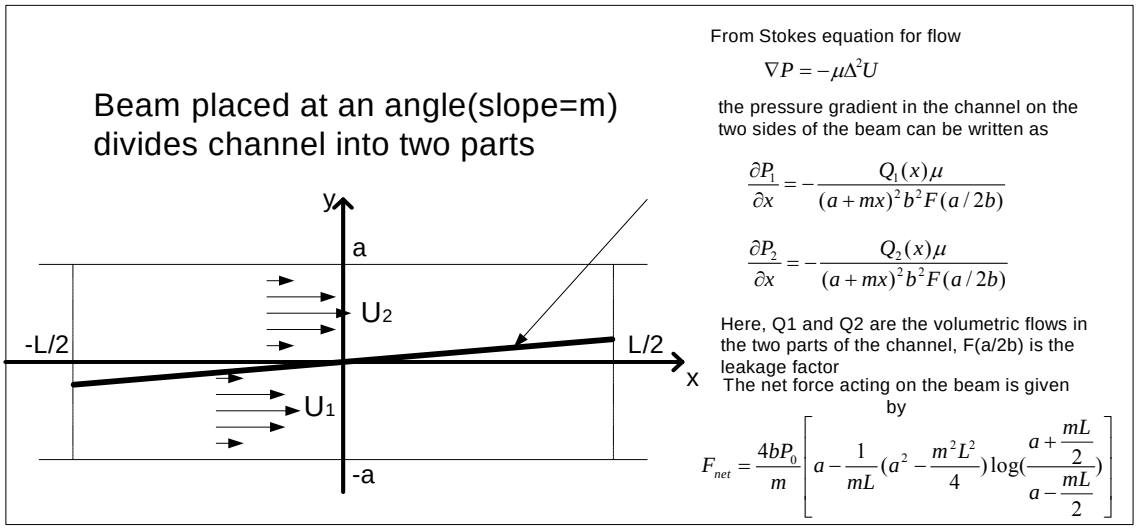

Figure 4.3 Analytical Model Developed For the Cantilever Beam Flow Sensor

Figure 4.4 Channel Structure for Testing, Stereo Lithography Fabricated Device

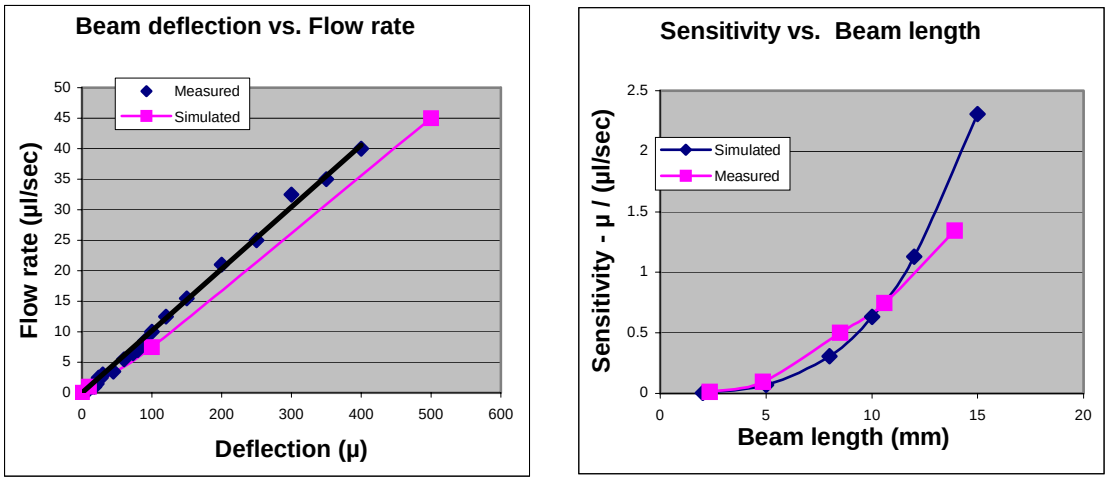

Figure 4.5 Comparison of Simulated and Measured Beam Deflection and Sensitivity

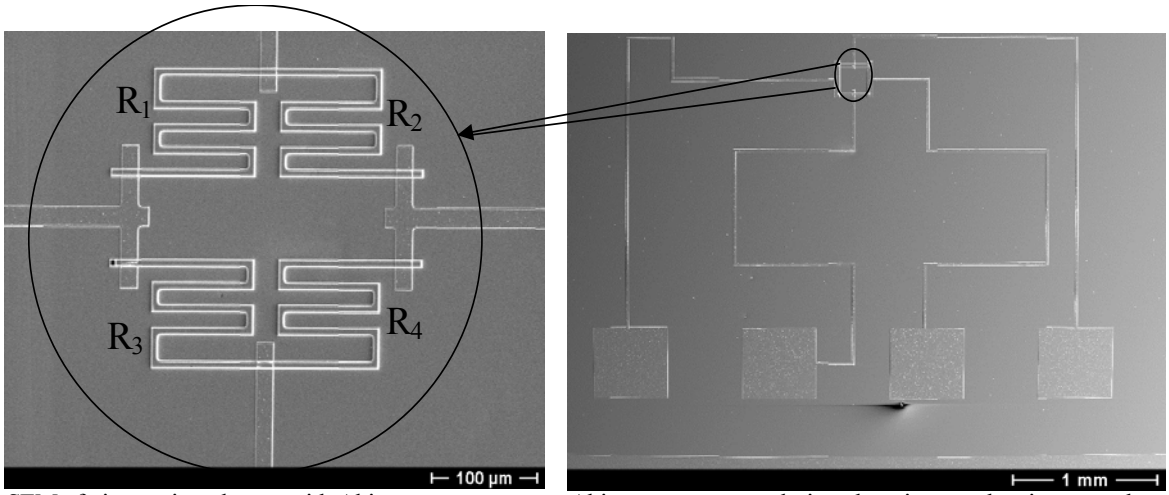

SEM of piezoresistor layout with Al interconnects Al interconnects are designed to give equal resistance values

Figure 4.6 SEM of Piezoresistor Layout

5 Elastic Feedback System for Needle Insertion and Fluid Sampling

The goal of this project was to provide a stage for mounting the hypodermic needles for skin penetration and incorporation of the ultrasonic capillary pump for ISF/blood sampling. No human testing was performed.

A vertical insertion stage was designed for insertion of a fixed length of micro needle into skin (**Figure 5.1**). The original needle array was to be mounted on the tip of a silicon beam and the force against skin was to be applied by driving the silicon beam in bimorph mode. This design possessed a few difficulties. First, the fabrication and assembling of micro needle arrays was complex and though skin penetration by micro needle arrays is a topic of active research now, it is far from a mature technology and would have added extra time to the accomplishment of this project. Second, incorporation of pumping and fluid transport mechanisms developed by the other subprojects was difficult. Based on this situation and the results from related subprojects, a new parallel insertion stage with elastic feed back was designed.

Feedback System Design

The elastic feedback needle stage is shown in **Figure 5.2**. This prototype stage was made in wood and elastic rubber bands. The rubber bands provided elastic feedback and adjustment of the force applied on the needle as it proceeded against the skin, resembling the adjustment in hand operated needle insertion: increased force when the skin resists the needle and decreased force when the skin is penetrated by the needle.

Figure 5.2 illustrates the configuration of the needle stage and feedback system. Solid plate 1 (5cm*2.5cm*0.3cm) was shaped into a rectangular frame. Solid plate 2 (4cm*1.5cm*0.3mm) was placed into this frame and could glide back and forth. Two rubber bands (5 and 6) were wrapped on the small extending parts on each longer side of plate 2 and then wrapped on plate 1, thus attaching plate 2 to frame 1 but not fixing the position of plate 2 relative to the frame. Screw 4 was at the end of frame 1 and screwing it in pushed forward plate 2, inserting the attached needle into the skin while stretching rubber bands 5 and 6 at the same time. Screwing out screw 4 released the rubber bands and the restoring force pulled the needle backward out of the skin. Hypodermic needle 8 was glued and then fixed on solid plate 3 by screw 11. Plate 3 was attached to plate 2 through rubber band 7 in a similar manner as plate 2 was attached to plate 1. The rubber band on plate 3 provided the elastic feedback when the needle came in contact with the skin.

When plate 2 moved forward to bring the needle tip into contact with skin surface, the resistance of the skin caused rubber band 7 to be stretched backward. The restoring force of the rubber band 7 increased as the resistive force of the skin increased. Once the skin was penetrated there was a sudden release of the resistive force, and the rubber band 7

was released correspondingly and thus decreased the pushing force on the needle. Therefore, the needle would not keep proceeding after the skin was penetrated, as in the case of a constant force driven needle without feedback control. Screw 12 on plate 2 was used to adjust the angle of the needle against skin.

Results

Conventional stainless steel hypodermic needles can be used in this design. A glass capillary was connected to the needle and driven ultrasonically with an attached piezoelectric PZT plate to pump fluid. Some results and discussions of this device are listed below.

1. The stage with needle and pump was designed so it could have been bonded to the forearm, or some other convenient place, to perform insertion and sampling.
2. An ultrasonic glass capillary pump was studied. The emphasis was on incorporation of the hypodermic needle and capillary pump. The combination of the two as illustrated in **Figure 5.2** was shown to pump water successfully.
3. The ultrasonic capillary pump workd by atomization and acoustic streaming. Both pumping of water accompanied by strong atomization at the opening of the capillary and pumping realized through continuous up flow of water were observed. However, since the lower part of the capillary was confined inside the needle and its mechanical conditions there vary easily, the atomization mechanism was more reliable and repeatable.
4. Pumping worked most effectively at ~450 kHz with 10Vpp driving voltage. The exact working frequency varied slightly from run to run or during continuous pumping.
5. The capillary effect was essential for the fluid to fill up the glass capillary before atomization at the opening started and continuous pumping of the fluid up the capillary channel occured. Sometimes, when the capillary force itself was not enough to pull the fluid up the channel, injection of fluid was needed to fill the channel of the capillary.
6. The fluid environment under the surface of human skin can be described as having negative pressure. It was unlikely the ISF would automatically fill the capillary by capillary effect. Investigation is still needed to determine whether the pressure gradient established by atomization at the opening is enough to pull fluid up the capillary channel, even with injection to fill the capillary beforehand.

Future Work

1. At the writing of this report, a collaboration with *Becton, Dickinson and Company* is in process to conduct in vivo animal experiments on needle insertion and ISF/blood sampling.
2. Design and expansion of the system to include the bioassay system and other components of the BioFlip project is the next step. **Figure 5.3** shows one possible design that can be realized with plane springs made by plastic molding or lithography.

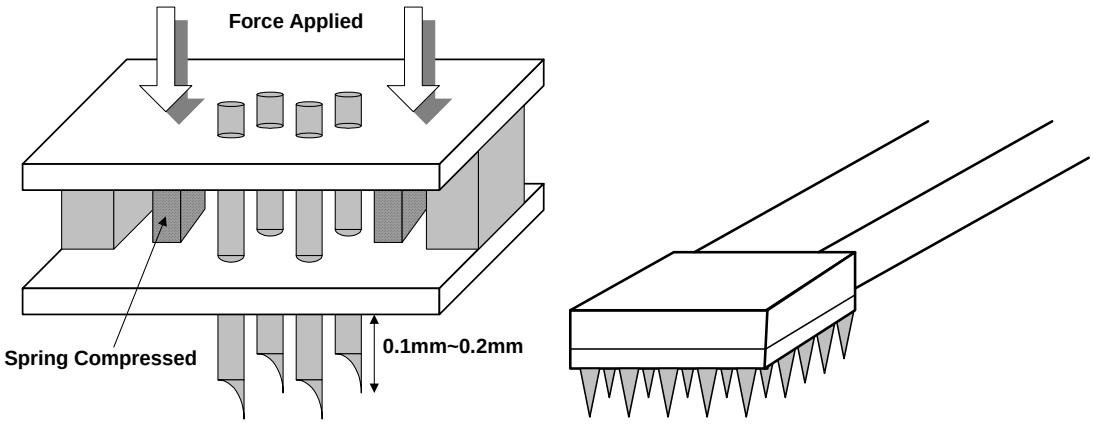

Figure 5.1 Vertical Insertion of Micro-Needle Array

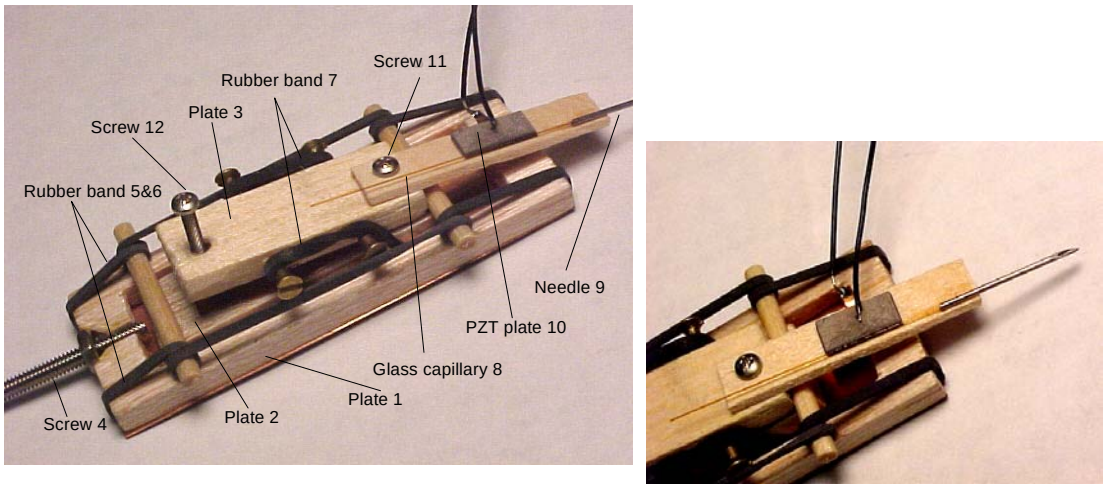

Figure 5.2 Needle Stage with Elastic Force Feedback and Ultrasonic Capillary Pump (23 gage stainless steel hypodermic needle, 200μmOD, 100μmID glass capillary and 4mm*8mm*0.5mm PZT5 plate)

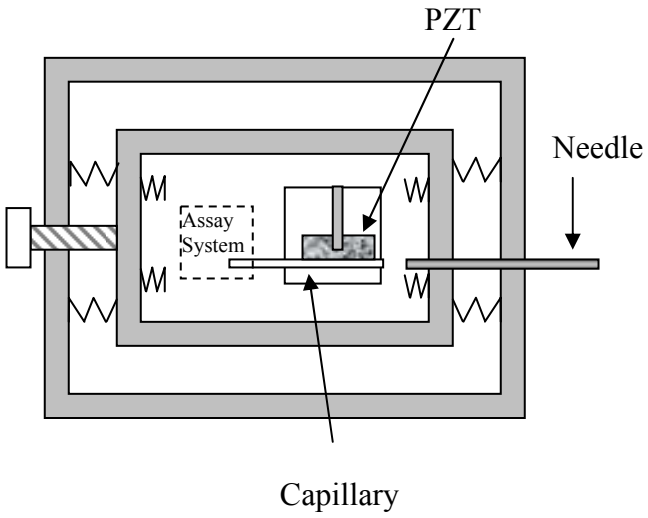

Figure 5.3 A Potential Redesign of the Needle Insertion and Pumping System

6 Ultrasonic Separations and Pumping in Glass Capillary System

The pump project led to ultrasonic separations that hold great promise for fast-integration of bead-based assays on the BioFlip platform. There is a need to separate different sized polystyrene beads coated with different antibodies and determine the size ratio in miniature biochemical systems. A typical electro-osmotic micro-fluidic assay system is shown in **Figure 6.1**. Microfluidic devices utilizing differential mobility in a high electric field for beads/molecules require a conducting medium. However, uncertainty in medium conductivity requires accurate arrival time of particles to be detected at the fixed optical detection system. Projected acoustic fields were used to solve this problem.

Bead separation and particle manipulation with a projected acoustic field was investigated by many other workers. Acoustic radiation forces generated by a concave transducer were used to concentrate particles at pressure nodes. Previous attempts for focusing beads at nodes using ultrasonic radiation force led to improved detection limits for agglutination assays. However, separation of different sizes using the acoustic radiation force was not demonstrated. The diffracted acoustic field from a particle leads to a non-symmetric acoustic field around the particle.

The physical location of nodes/antinodes in standing waves is usually sharp leading to beads clustering around a point and making separation of different size particles difficult. However, if one can widen the nodes/antinodes one can expect a gradient of the radiation force acting on the mixed beads leading to separation between different size beads at the broad nodes/antinodes. Furthermore the locations of the beads are predictable and stable so that an optical detector can be placed to gather information for assays at the nodes/antinodes rather than across the entire glass loop, (**Figure 6.2**).

In addition to the effects of radiation pressure, the volume uptake of the particles in finite space of a glass capillary will lead to broadening of the bands formed by the beads. Since the force is proportional to the particle diameter cubed, one predicts that the large particles will move towards the antinodes with higher force leading to particle separation. Additionally, there is also a shear viscous acoustic field near the wall of the glass capillaries. This field causes acoustic streaming flow.

Beads in the acoustic field will move into nodes or antinodes depending on the sign of the acoustic contrast factor (F). If the F is positive, beads move toward the antinodes and if F is negative beads move toward the nodes. The density of the bead and speed of sound in the bead help determine the acoustic contrast factor. Values for polystyrene resulted in a positive sign of the acoustic contrast factor causing the beads to move towards the antinodes.

Pump Design

A schematic drawing of the glass capillary/PZT transducer is shown in **Figure 6.3**. A polyimide coated glass capillary (Inside Diameter = 100 μm, Outside Diameter = 200 μm, polyimide thickness = 12 μm) was folded around the PZT plate (10 mm x 2.5 mm x 0.5 mm) with a knot. The knot acoustically decoupled capillary modes from the inlet/outlet ends of the capillary so that any micro-fluidic boundary conditions could be applied to the system. For intimate contact, the glass capillary was adhesively bonded to edges of PZT plate using cyanoacrylate. A typical hand-assembled device is shown in **Figure 6.4**. Two electrodes were soldered at the center of the PZT plate since a node of the displacement of PZT plate was at the center.

Results

There were two half-wavelength vibration modes of the PZT plate, namely the length mode and width mode (which was weakly coupled to bending modes) as shown **Figure 6.5**. Since these modes corresponded to half-wavelength vibration, the two resonance frequencies were 160 kHz and 640 kHz respectively. Electrical impedance measured with an impedance analyzer is shown in **Figure 6.6**.

A mixture of different size polystyrene beads was prepared for the separation experiment. As mentioned earlier, the polystyrene beads subjected to the acoustic field moved into antinodes due to the density-compressibility factor regardless of size difference. However, the radiation forces on the beads were proportional to the radius of the bead. Due to the different radiation force and gradient of the radiation force in the antinodes, beads that moved to antinodes were separated by size.

Separation of beads at an antinode is shown in **Figure 6.7**. The diameter of red fluorescence colored beads was 1 μm and that of green fluorescence colored beads was 5 μm. The driving voltage was 3 Vpp and the driving frequency was 160 KHz. As resonance frequency increased, such as higher harmonics of the length modes or width modes, the broad band became sharp leading to difficulty in the separation process. Furthermore, the driving voltage had to be increased up to 7 Vpp for effective separation.

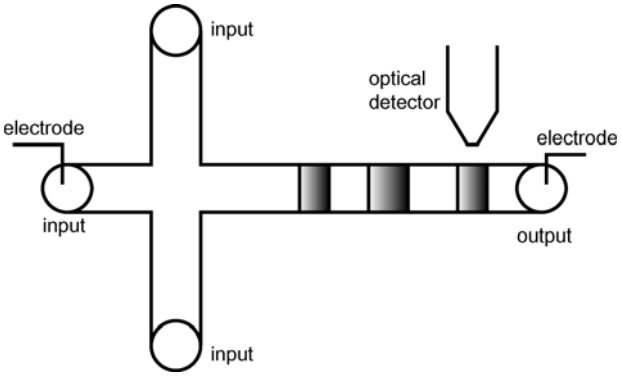

Figure 6.1 A Typical Electro-Osmotic Micro-Fluidic Assay System.

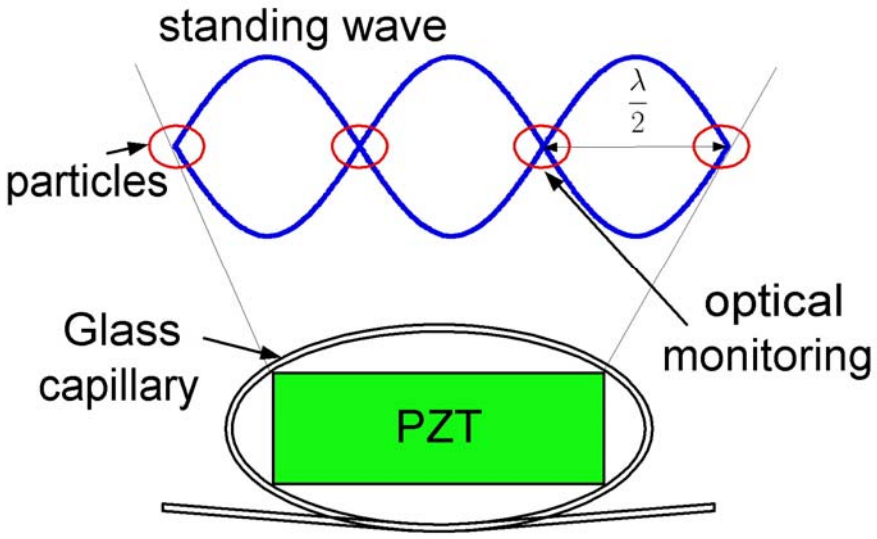

Figure 6.2 Node/Antinode Separation in Capillary

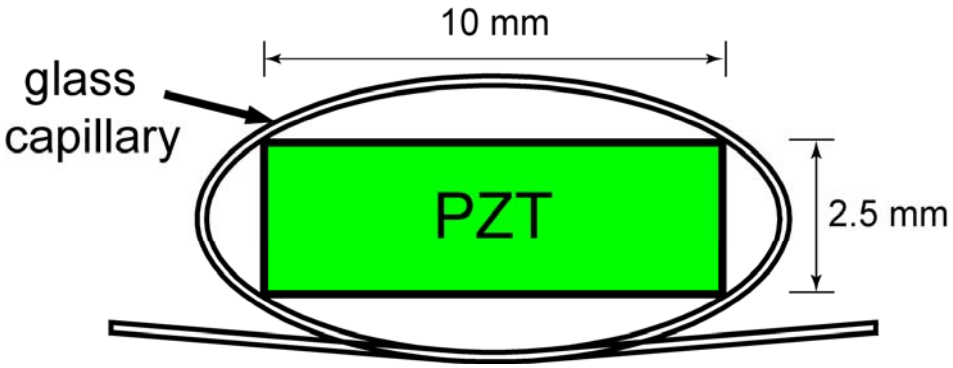

Figure 6.3 A Schematic Drawing of the Glass Capillary/PZT Transducer

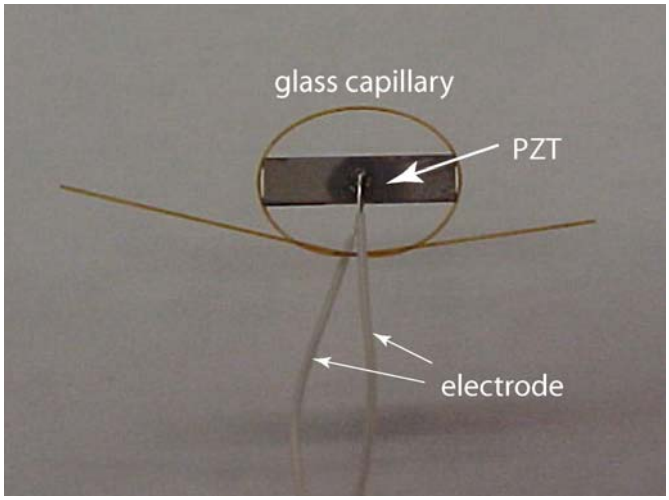

Figure 6.4 The Capillary/PZT Transducer with Electrodes.

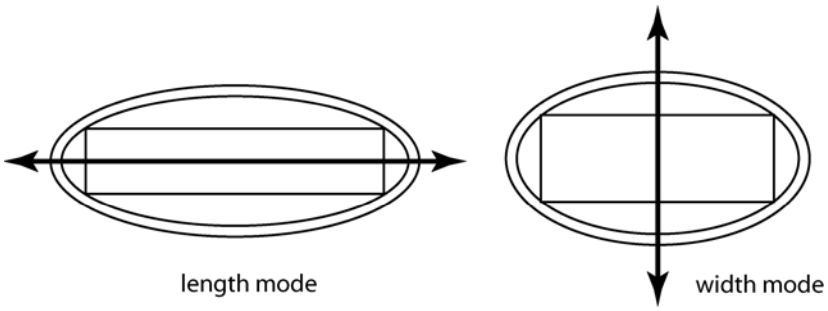

Figure 6.5 Two Half-Wavelength Vibration Modes of the PZT Plate.

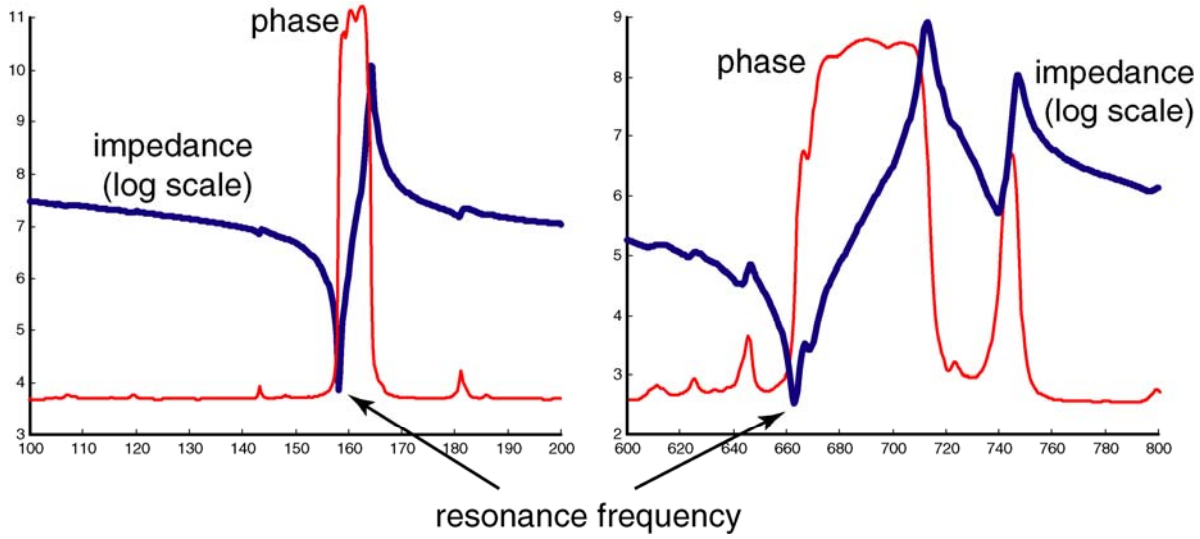

Figure 6.6 Measured Impedance of the PZT/glass Transducer: Left figure shows resonance frequency of the length mode (frequency: 160 kHz) and right shows resonance frequency of the width mode (frequency: 640 kHz).

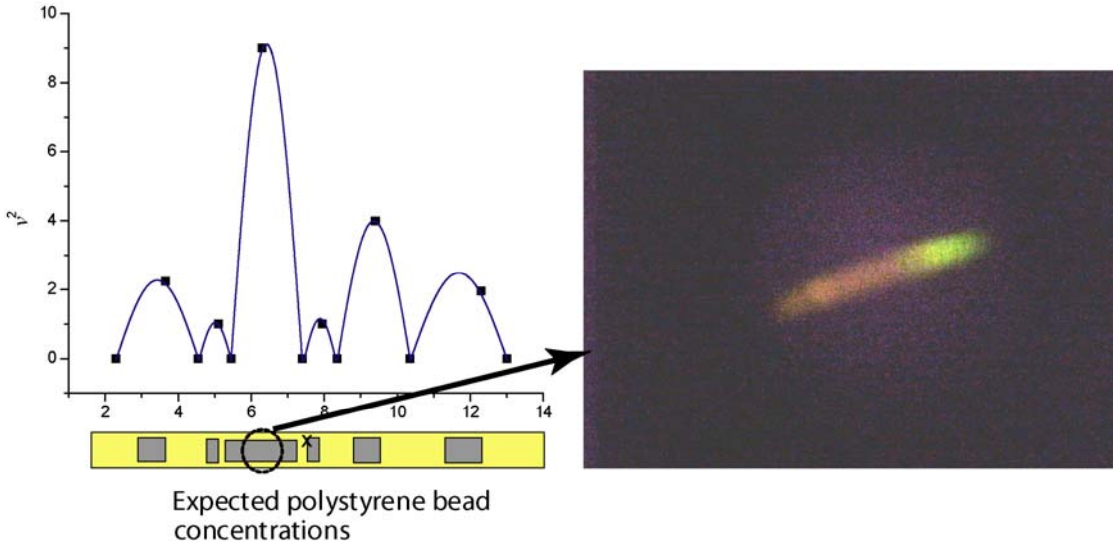

Figure 6.7 Bead Separation at a Broad Antinode: The size of the beads on left side is 1 μm and the size of the beads on right side is 5 μm.

7 Separation of Microparticles Using an Ultrasonic Standing Wave Field

The overall goal of this sub-project was to use computer simulation techniques to study the separation of mixtures of microparticles in the presence of an ultrasonic standing wave field. An example use is analysis of white blood cell count. A white blood cell count can be used to determine the health of a patient. If white blood cells could be extracted from a blood sample obtained by the microfluidic system, optical detection methods could then be used to perform a count.

This project used ultrasonic waves to create such a separation. Understanding the dynamics of binary systems was the first priority. Special attention was paid to the behavior of particles trapped by individual acoustic pressure nodes. It was also desirable to know how acoustic intensity and particle size contrast influence separation.

A second goal of the project was to assess the feasibility of a new separation technique loosely termed acoustic chromatography, performed experimentally by first injecting the mixture into a microcapillary. Next, an ultrasonic standing wave was established in the axial direction. Finally, a motorized microliter syringe drove the fluid through the capillary. The acoustic force hindered the translation of the larger size particles more so than the smaller particles. This resulted in the smaller particles having a greater average velocity. A separation took place once given sufficient time. This model considered acoustic, viscous, excluded volume, and Brownian forces.

A separation technique is only useful to the lab-on-a-chip community if it can be performed over small length scales. The aim of this work was to accomplish the same result as in the previously described acoustic chromatography but on a length scale of a few acoustic wavelengths. Two methods were developed that meet this criterion. The first method required choosing the acoustic parameters such that the larger particles were trapped at the first few acoustic pressure nodes. This method required careful selection of the acoustic intensity, acoustic wavelength, and average fluid velocity. The second method involved adding at third component consisting of particles that were much larger in size than the largest size particle in the binary mixture. When introduced to the acoustic field these much larger particles migrated to the nearest pressure node where they arranged into an array. Particles whose diameter was less than some cutoff value may pass through the cavities in this array. Essentially, the third component organized into a microscopic, semi-permeable mechanical filter. This technique provided separation on a length scale of less than an acoustic wavelength.

It was desired to simulate the motion of non-spherical particles undergoing acoustic chromatography. A goal of the project was to separate doublets or tangent-sphere dumbbells from single spherical particles. If such a separation were possible it would allow for the detection of nano-molar concentrations of proteins or macromolecules. This

analytical technique was conducted by adding latex spheres (coated with specialized antibodies) to the solution containing the antigen. Biomolecules containing two antigenic sites of differing type will each chemically bond to corresponding antibody-coated spheres. After sufficient time has occurred for mixing, the solution consists of single spheres whose antibody coating has not reacted and doublets or complexes formed from two spheres whose antibody coating has reacted. Acoustic chromatography may then be used to separate the mixture. A count can be performed upon purification and (a) the presence of an antigen can be tested for or (b) the concentration of a particular antigen can be determined.

Results

Figure 7.1 is an image from a simulation of 1 and 2 μm particles after separation about a single acoustic pressure node. It was seen that the larger particles, which experienced the greater acoustic force, were positioned closest to the node. Due to excluded volume effects the smaller particles were displaced to the outside.

The idea of a microscopic mechanical filter was explored using particles of 30 μm in diameter. Separation of a mixture of 1 and 5 μm diameter particles using the filter was attempted. **Figure 7.2** is an image of the simulation.

The direction of flow in **Figure 7.2** is from left to right. The large green particles were responsible for creating the filter. During the course of the separation their positions were approximately constant. The image revealed that the 5 μm particles were trapped by the array whereas the 1 μm particles snaked through void pathways in the filter.

After enough data was acquired, mixing fraction diagrams were constructed for the intra-node separation work. Mixing fraction is a measure of the overlap between layers or bands, which occur on either side of the pressure node. When the particle sizes are similar the mixing tends to be high. **Figure 7.3** and **Figure 7.4** illustrate this trend for systems of 1 and 1.25 μm particles and 1 and 1.50 μm particles, respectively:

On comparison of **Figures 7.3 & 7.4**, band resolution is higher in **Figure 7.4** (where there is a greater difference in the size of the particles). It is important to know how the mixing fraction varies with particle size contrast.

Figure 7.5 is a mixing fraction plot for a base particle size of 1 μm. It is seen from **Figure 7.5** that as the size ratio approached unity an appreciable separation did not take place. As the size ratio increased from unity the separation sharpened.

Through simulation the required time to separate a mixture of particles in the continuous flow process was determined (i.e., acoustic chromatography). The trajectories of particles flowing in a microcapillary, subject to the effects of a standing wave established in the axial direction, were simulated. A system was modeled where the wavelength was 1 mm,

acoustic intensity of 0.1 W/cm^2, average fluid velocity of 0.01 mm/s, and the radius of the capillary was 37. 5 μm. The 1200 particles of three different sizes were tracked for 89.5 hrs. in real time. The concentration and average position of the particles is shown in **Figure 7.6**.

The results indicated that the 1 and 3 μm particles completely separated from the 5 μm particles. Eventually the 1 μm particles separated from the 3 μm particles yielding complete purification.

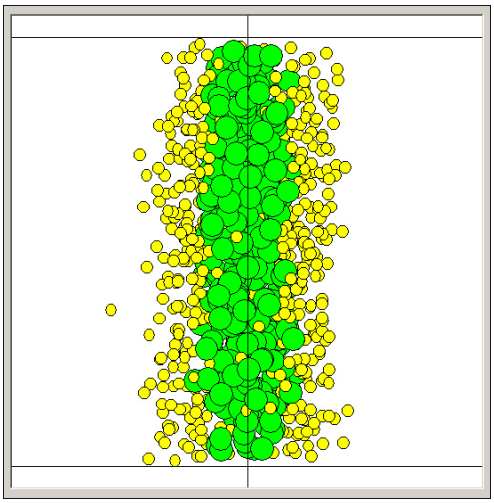

Figure 7.1 Intranode Separation

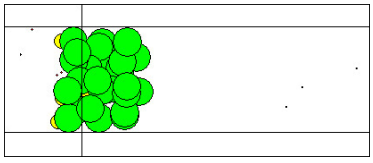

Figure 7.2 Acoustic Filter

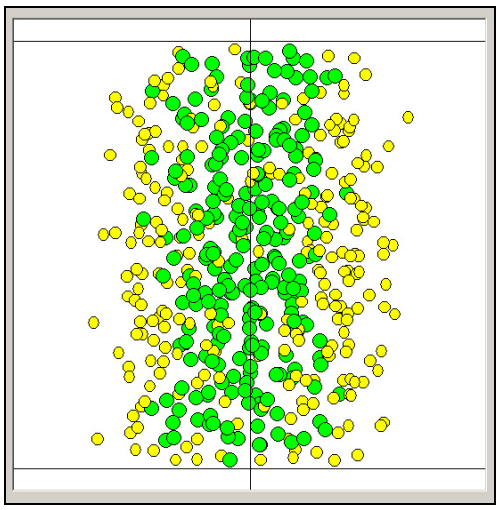

Figure 7.3 Separation for Particle Sizes = 1,1.25 μm

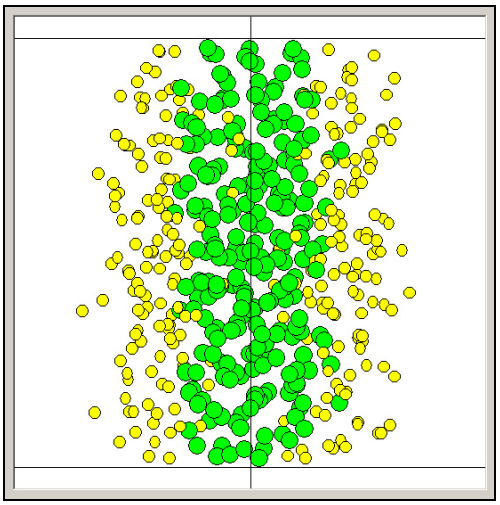

Figure 7.4 Separation for Particle Sizes = 1,1.5 μm

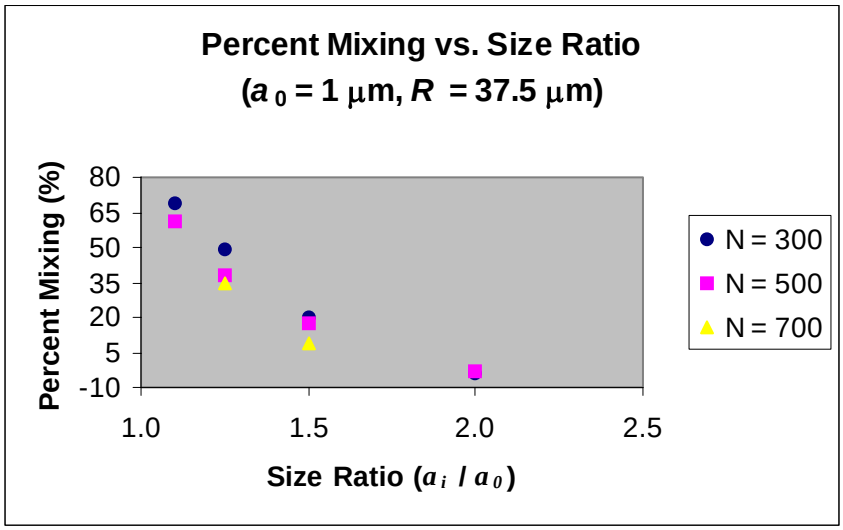

Figure 7.5 Mixing Fraction Diagram

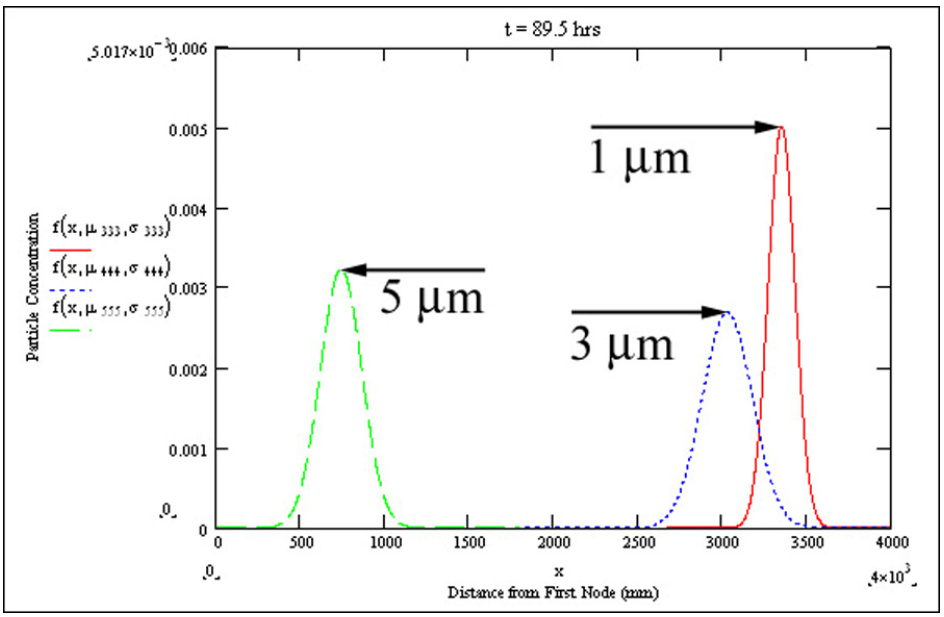

Figure 7.6 Acoustic Chromatography

8 Sensing Protein Conformational Changes with Resonant Antennas

Determining changes in the conformation of proteins in solution is necessary for a variety of applications, including folding/unfolding thermodynamics and kinetics, enzyme catalysis and ligand binding. Water may be used as a reporter molecule for protein conformational changes. The use of a resonant planar slot antenna to measure perturbations of the dielectric properties of water was proposed. Changes in permittivity within the near-zone of the antenna are reflected as shifts of the antenna's resonant frequency, which can be adjusted by changing the dimensions of the slot. Conformational change as determined by permittivity changes can be related and compared to conformational changes determined by other methods, such as UV/VIS (ultra violet / visual spectrum) or fluorescence spectroscopy.

Results

A co-axial fed resonant slot antenna suitable for measuring changes in the conformation of proteins in solution was designed, built, and tested. This antenna was fixed to the exterior of a fused quartz cuvette, allowing simultaneous microwave and UV/VIS spectroscopic measurements. Typical spectra obtained using these antennas are shown in **Figures 8.1** and **8.2.**

Changes in permittivity within the antennas near zone, thought to be due to release or re-organization of water shells surrounding the protein, are reflected as shifts in the antennas resonant peaks. The spectra in the frequency domain may be fitted to multiple Lorentzian peaks. Initial results indicated that the thermal response of these peaks yielded sigmoidal curves typical of cooperative unfolding. Such a sigmoidal response was absent when a solution of buffer alone was heated under the same conditions, (**Figure 8.3**).

Bovine pancreatic ribonuclease A (RNase A), a small globular protein, was used for all experiments in a solution of 30 mM sodium acetate/acetic acid, 100 mM sodium chloride, pH 4.5. The positions of peaks in the microwave spectra were shown to vary approximately linearly with protein concentration.

Thermal unfolding of RNase A was repeated multiple times, at concentrations varying from 0.2 to 1 mg/mL (14.6 to 73.0 μM), (**Figure 8.4**). Midpoint temperature (T_m, defined as the temperature at which 50% of the protein molecules are folded) and unfolding enthalpy (defined as the heat released upon unfolding 1 mole of protein) were invariant with protein concentration, (**Figure 8.5**). After obtaining peak positions by fitting peak spectra to Lorentzian peaks (**Figure 8.6**), peak positions as a function of temperature were fitted to a two-state unfolding model (**Figure 8.7**). These curves yielded values of midpoint temperature (T_m) and unfolding enthalpy (ΔH_m) very similar to those results obtained from UV/VIS spectroscopy alone. These T_m and ΔH_m values, shown in **Table 1**,

also compare well to those obtained by other researchers. All experiments were performed at a low power range (-15 to +5 dB).

Table 1 Results of Fitting of Data from Microwave and UV/VIS Measurements to 2-State Unfolding Model.

	ΔH_m (kcal/mol)	T_m (°C)
Microwave (all peaks)	54.3	55.2
UV/VIS	61.3	59.2

Future work

Several important questions remain to be answered:

1) *Dependence of unfolding results on microwave power*: Although initial results indicated that the protein was not destabilized by the presence of microwave radiation, additional experiments are needed. Unfolding at a single protein concentration will be repeated at a variety of power settings. It is expected that midpoint temperature T_m and unfolding enthalpy ΔH_m will not depend on microwave power.
2) *Effect of microwaves on enzyme activity:* RNase A is an enzyme that cleaves single-stranded RNA in solution. This reaction can be monitored using UV/VIS spectroscopy. Two questions can be answered here. First, can the activity of RNase A and/or the cleavage of RNA be detected using our antenna system? Second, does microwave power have any effect on the rate or efficiency of cleavage?
3) *Detection of protein-ligand association:* Using a non-hydrolysable RNA analog, we will attempt to detect the binding of RNA to RNase A. In addition, the binding of ribonuclease inhibitor (RI) to RNase A can also be detected. RI binds tightly to RNase A and inhibits its enzymatic functions.
4) *Other proteins and/or biological molecules:* The system in this study can be extended to the study of other proteins and other biological systems (hybridization of DNA/RNA, melting of lipids, etc.).

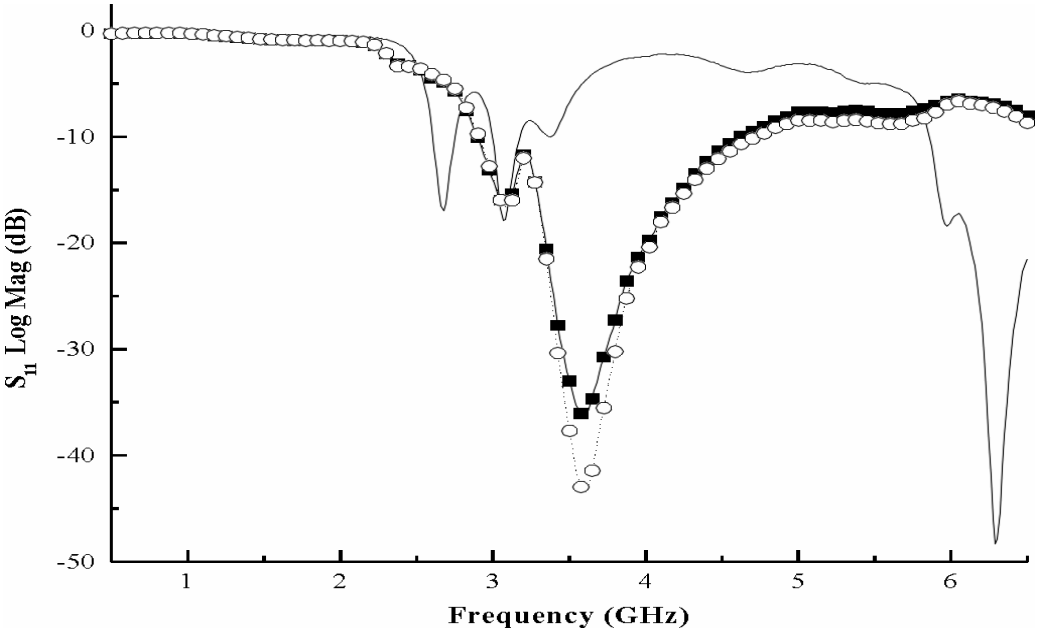

Figure 8.1 Frequency Response of Air (solid line), Buffer (■), and RNase A (○) as Measured on a Network Analyzer

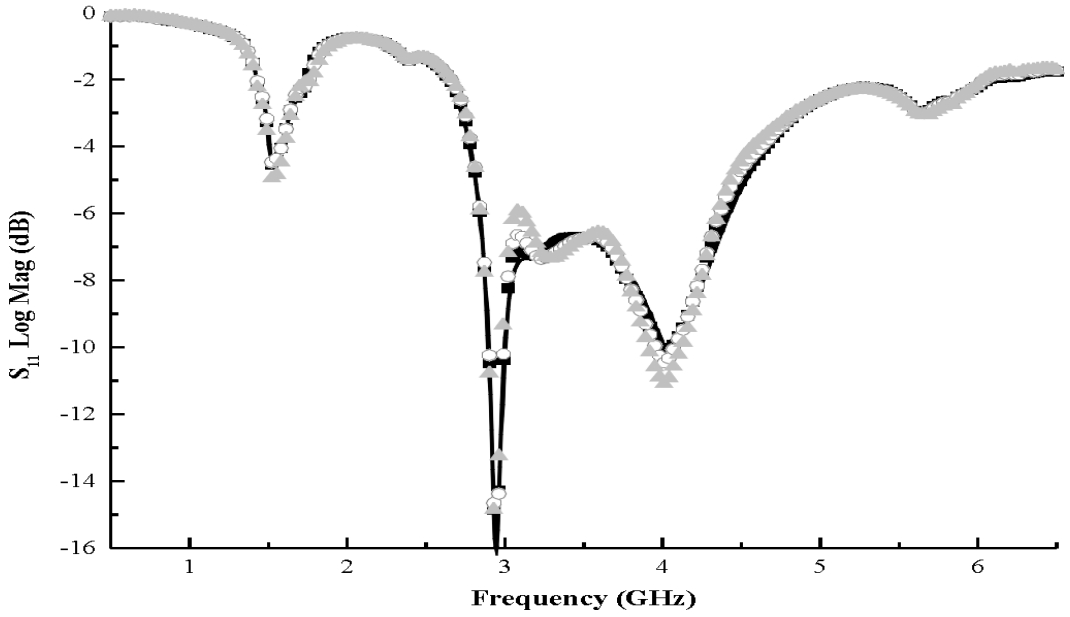

Figure 8.2 Frequency Response of RNase A at Selected Temperatures. Symbols: 34.8 ºC (solid line), 45.6º C (■), 54.5 ºC (○), 65.5 ºC (▲)

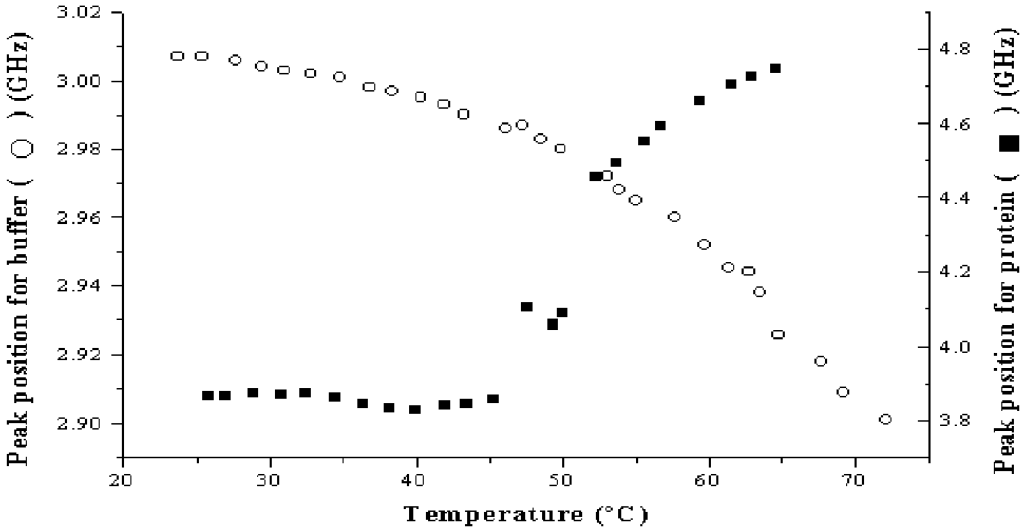

Figure 8.3 Results of Fitting of Representative Peaks from Buffer (○) and Protein Solution (■). Note that protein peaks form a characteristic sigmoidal curve.

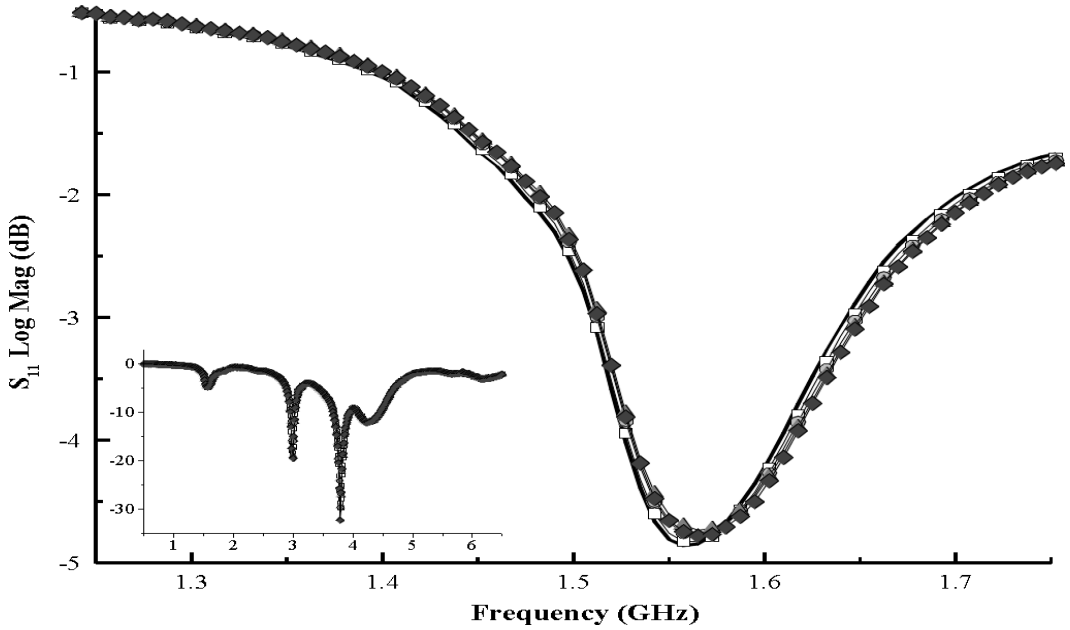

Figure 8.4 Variation of Peak Position with Concentration of RNase A. Inset shows complete spectra; close-up of a single peak is shown in the larger image. RNase A concentrations (mg/mL): 0 (solid line), 1.18 (□), 2.08 (●), 2.79 (◆), 3.35(▲)

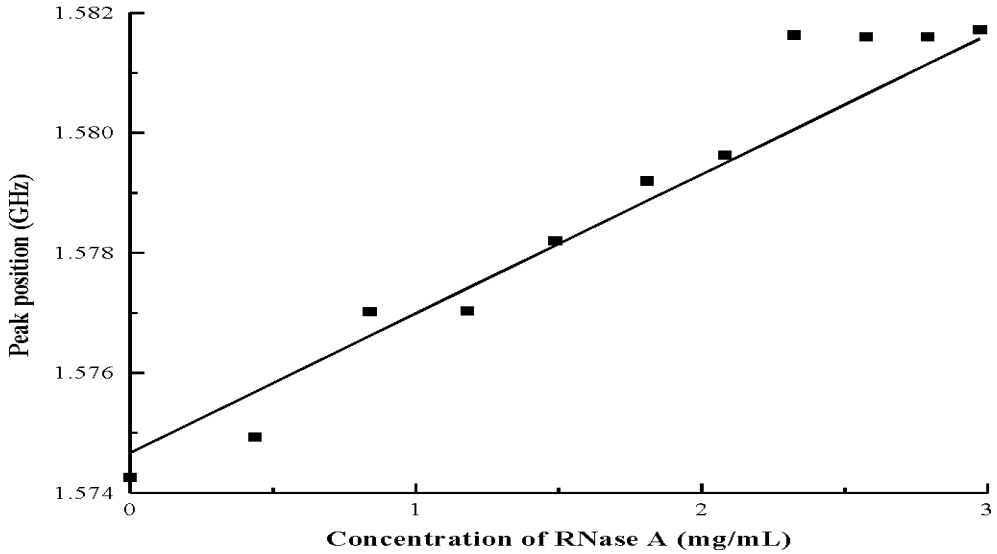

Figure 8.5 Variation of Peak 3 with RNase A Concentration. Solid line indicates linear fit to data, with slope 2.75 MHz mg-1 mL, intercept 1.57 GHz and R 0.984.

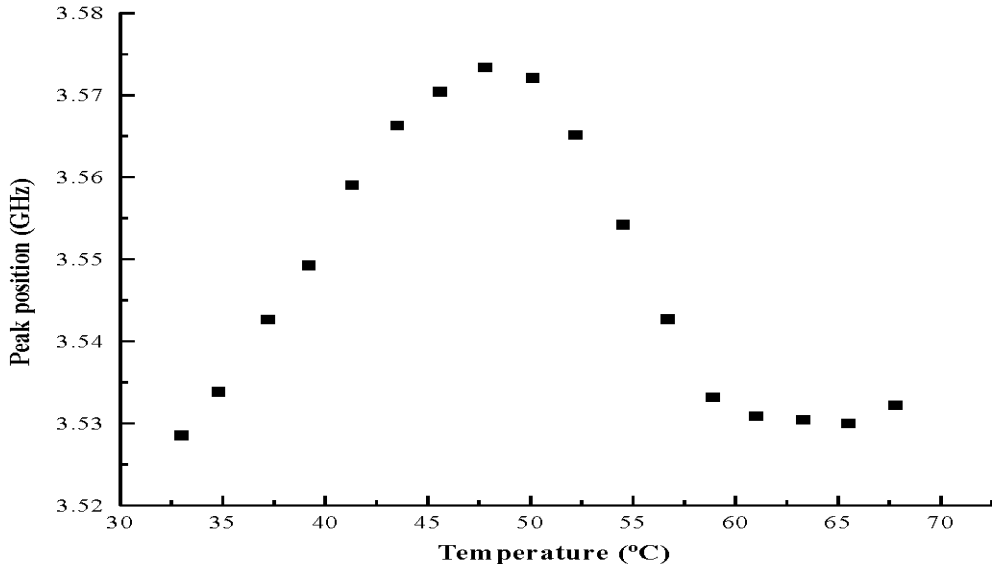

Figure 8.6 Variation of Position of Peak 5 with Temperature.

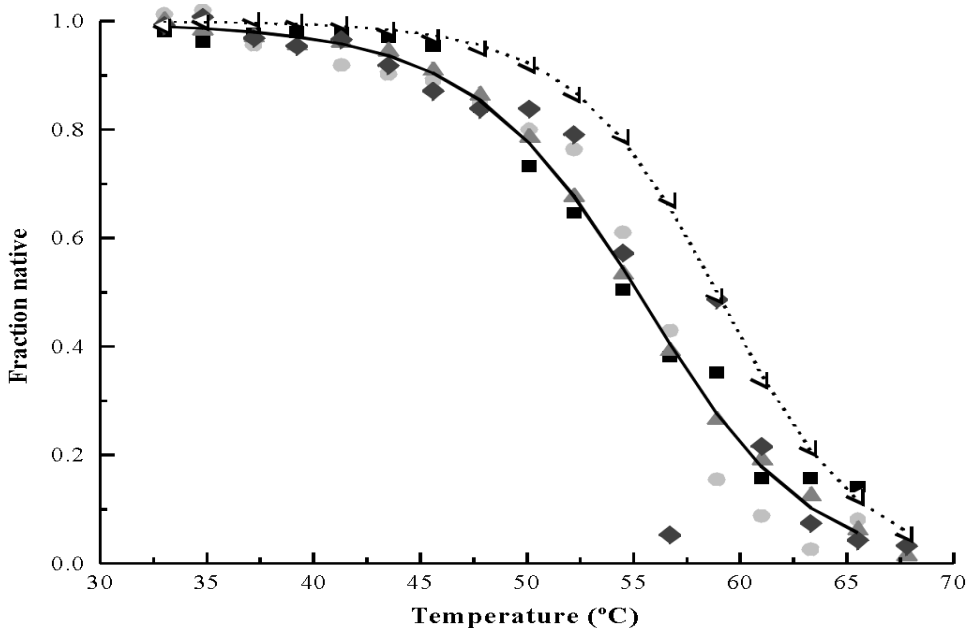

Figure 8.7 Fit of Data from Microwave and UV/VIS Measurements to 2-state Unfolding Model. Microwave data: peak 1 (■), peak 4 (●), peak 5 (▲), peak 7 (◆), fit to all peaks (solid line). UV/VIS data: data (◁), fit (dotted line).

Bibliography

1. Araz, K., Lee, C.H., Lal, A., “Finite Element Modeling of Ultrasonic Separation at the Microscale”, IEEE UFFC Proceedings, Montreal, 2004
2. Ardanuc, S., Lal, A., “PZT Driven, Micromachined, 2-D Membrane Arrays,” IEEE UFFC Proceedings, Montreal, 2004
3. Chen, X., Lal, A., Riccio, M, Gilmour, R.G., “Cardiac Signal Recording Using Ultrasonic Silicon Microprobes,” Proceedings of the Solid State Sensor and Actuator Workshop, Hilton Head Island, South Carolina, 2004
4. Araz, M.K., Lee, C. H., Lal, A., “Ultrasonic Separations in Microfluidic Capillaries,” Proceedings of the IEEE-UFFC Conference, Hawaii, 2003 : WINNER of the best student paper in the industrial applications division
5. Sathaye, A., Lal, A., “An Ultrasonic Micromachined Integrated Capacitive Sensor for Biological Sample Preparation On a Microfluidic Platform,” Proceedings of the IEEE-UFFC Conference, Hawaii, 2003
6. Duggirala, R., Lal, A. “A Pyroelectric -Piezoelectric Valve for Integrated Microfluidics,” Digest of Technical Papers, The 12th International Conference on Solid State Sensors, Actuators and Microsystems, Transducers’03, Boston, pp. 55-58
7. Radhakrishnan, S., Lal, A., “A Drag Force Flow Sensor For Closed-Loop Flow Control,” Proceedings of the IEEE MEMS 2003, Kyoto, pp.307-310
8. Sathaye, A., Lal, A., “Numerical Simulation Of Acoustic Streaming Near Embedded Microstructures Inside Microfluidic Channels,” Proceedings of the IEEE-UFFC Conference, Munich, 2002
9. Kan, S., Lal, A., “Control of Bulk Driven Ultrasonic Surface Micromachined Resonator,” Proceedings of the IEEE-UFFC Conference, Munich, 2002
10. Kaajakari, V., Lal, A., “Parametric Excitation of Whispering Gallery Modes on Circular Micromachined Plates,” Proceedings of the IEEE-UFFC Conference, Munich, 2002
11. Lee, C., Lal, A., “Low-Voltage High-Speed Ultrasonic Chromatography For Microfluidic Assays,” Proceedings of the Solid State Sensor and Actuator Workshop, Hilton Head Island, South Carolina, 2002, pp. 206-209
12. Siwapornsathain, E., Lal, A., Binard, J., “Telemetry and Sensor Platform for Ambulatory Urodynamics”, Proceedings of the 2nd Annual International IEEE-EMBS Special Topic Conference on Microtechnologies in Medicine & Biology, Madison, WI., pp 283-287, May 2002
13. Son, I., Lal, A., “A Remotely Actuated Magnetic Actuator For Microsurgery With Piezoresistive Feedback,” Proceedings of the 2nd Annual International IEEE-EMBS Special Topic Conference on Microtechnologies in Medicine & Biology, Madison, WI., pp 332-336, May 2002
14. Radhakrishnan, S., Solak, H., Lal, A., “In-Channel Flow Sensor Using Drag Forces,” Proceedings of the μTAS 2001 Conference, Monterey, CA, pp. 179-181, Kluwer
15. Sathaye, A., Lal, A., “An acoustic vortex particle concentrator,” Proceedings of the μTAS 2001 Conference, Monterey, CA, pp. 185-187, Kluwer

16. Lee, C., Dong, Y., Lal, A., “A glass-PZT Ultrasonic Microfluidics Platform,” Proceedings of the μTAS 2001 Conference, Monterey, CA, pp. 489-491, Kluwer
17. Siwaponrsathain, E., Lal, A., “Micromachined Ultrasonic Si/PZT Transducer for Underwater Communications,” IEEE Ultrasonics, Ferroelectrics, and Frequency Control Society Symposium, 2001, Atlanta
18. Guo, H., Lal, A., “Flexural Plate Wave Excitation Using Bulk Modes,” IEEE Ultrasonics, Ferroelectrics, and Frequency Control Society Symposium, 2001, Atlanta
19. Guo, H., Lal, A., “Characterization of Silicon Nitride Membranes Using Resonant Ultrasound Spectroscopy,” IEEE Ultrasonics, Ferroelectrics, and Frequency Control Society Symposium, 2001, Atlanta
20. Siwaponrsathain, E., Lal, A., “Micromachined Ultrasonic Si/PZT Transducer for Underwater Communications,” IEEE Ultrasonics, Ferroelectrics, and Frequency Control Society Symposium, 2001, Atlanta
21. Kaajakari, V., Lal, A., “Optimization of a Bulk-Driven Surface Micromachined Ultrasonic Micromotor,” IEEE Ultrasonics, Ferroelectrics, and Frequency Control Society Symposium, 2001, Atlanta
22. Lee, C., Lal, A., “Glass Capillary/PZT Transverse Wave Actuator for Microfluidic Radiation Force Assay,” IEEE Ultrasonics, Ferroelectrics, and Frequency Control Society Symposium, 2001, Atlanta
23. Sathaye, A., Lal, A., “An acoustic vortex generator for microfluidic particle entrapment,” IEEE Ultrasonics, Ferroelectrics, and Frequency Control Society Symposium, 2001, Atlanta
24. Ochoco, J., Lal, A., “Programmable Acoustic Streaming on a 2D PZT Pixel Array,” IEEE Ultrasonics, Ferroelectrics, and Frequency Control Society Symposium, 2001, Atlanta
25. Ochoco, J., Lal, A., “Resonance Frequency Tuning of Two-Dimensional PZT array using Laser Trimming,” IEEE Ultrasonics, Ferroelectrics, and Frequency Control Society Symposium, 2001, Atlanta
26. Chen, X., “Integrated Pressure and Flow Sensor in Silicon-Based Ultrasonic Surgical Actuator,” IEEE Ultrasonics, Ferroelectrics, and Frequency Control Society Symposium, 2001, Atlanta
27. Chen, X., Lal, A., “Micromachined Ultrasonic Ophthalmic Microsurgical tool with integrated Pressure sensor,” Digest of Technical Papers, International Conference on Solid State Sensors and Actuators, Munich, pp. 424-427
28. Kaajakari, V., Sathaye, A., Lal, A., “A Frequency Addressable Ultrasonic Microfluidic Actuator Array,” Digest of Technical Papers, International Conference on Solid State Sensors and Actuators, Munich, pp. 958-961

Students

- Serhan Ardanuc – 2D Array
- Mehmet Kursad Araz – Acoustic Chromatography
- Chung-Hoon Lee – Separations and glass/capillary/PZT structures -ECE
- Xi Chen – Micro-needle work -ECE
- Jomar Ochoco – PZT arrays - ECE
- Shankar Radhakrishnan – Flow sensing -ECE
- Rajesh Duggirala – PZT micromachining – micro-valves - ECE
- Il-Seok Son – Piezoresistive sensors and extrusion - ECE
- Enny Kho – Sine wave generation – Undergraduate -ECE
- Abhijit Sathaye – Vortex particle collector - ECE
- Jon Haverlson – Ultrasonic separation modeling – Chemical Engineering
- Kimberly Taylor – RF detection of proteins- ECE

Acronyms

CFD	Computational Fluidic Dynamics
CFDRC	Computational Fluid Dynamics Research Corporation
CMOS	Complimentary Metal Oxide Semiconductor
CRP	C-reactive proteins
DAC	Digital to Analog Converter
GHz	Giga Hertz
FPGA	Field Programmable Gate Array
ISF	Interstitial Fluid
kHz	kilo Hertz
LCD	Liquid Crystal Display
MEMS	MicroElectricalMechanical Systems
MHz	Mega Hertz
mW	milli Watt
PDMS	Polydimethylsilane
PECVD	Plasma Enhanced Chemical Vapor Deposition
PI	Principal Investigator
PZT	Lead-Zirconate-Titanate
RF	Radio Frequency
SEM	Scanning Electron Microscope
Si	Silicon
SLA	Stereo Lithography
UV/VIS	Ultra Violet / Visual Spectrum
Vpp	Voltage peak to peak
2D	Two Dimensional